World Electric Vehicle Journal

MDPI

Article

A Novel Tri-Mode Bidirectional DC–DC Converter for Enhancing Regenerative Braking Efficiency and Speed Control in Electric Vehicles

Noah Dias *, Anant J. Naik and Vinayak N. Shet

Department of Electrical and Electronics Engineering, Goa College of Engineering, Ponda 403401, India
* Correspondence: noah@gec.ac.in

Abstract: A bidirectional dc–dc converter is used to match the voltage levels between a low-voltage battery and a high-voltage traction machine in an electric vehicle. Using a conventional bidirectional converter with a standard voltage range, there is a limitation to the fine variation in the electric vehicle speed. During the regenerative braking process, when the speed decreases below a certain value, the generated voltage is insufficient to charge the battery, hence the regenerated energy cannot be stored. This paper proposes a novel bidirectional converter featuring three distinct operational modes: boost, buck and buck-boost. In the normal driving mode, it operates as a boost converter, providing double gain and accommodating a wide voltage range. During regenerative braking, the proposed converter switches to the buck or buck-boost mode based on the control algorithm. This adaptation is intended to either decrease the generated voltage to charge the battery effectively or to raise the voltage if it is insufficient for charging the battery. This configuration provides voltage stress of half the dc link voltage on the switches. This paper provides a comprehensive analysis of the proposed circuit, a detailed description of the control strategy with pulse generation logic for all switches and a mode transition algorithm. The simulation results of a circuit operating at a 1500 W power level are presented and compared with those of a standard bidirectional converter.

Keywords: dc–dc converter; electric vehicle; non-isolated; bidirectional; controller; regenerative braking

Citation: Dias, N.; Naik, A.J.; Shet, V.N. A Novel Tri-Mode Bidirectional DC–DC Converter for Enhancing Regenerative Braking Efficiency and Speed Control in Electric Vehicles. *World Electr. Veh. J.* **2024**, *15*, 12. https://doi.org/10.3390/wevj15010012

Academic Editors: Jianfei Chen, Liyan Zhu, Chen Duan and Haibo Huang

Received: 23 November 2023
Revised: 15 December 2023
Accepted: 20 December 2023
Published: 2 January 2024

1. Introduction

The automobile industry is being revolutionized by electric vehicles (EVs), which are paving the way for a more sustainable future in light of recent technological developments and increased climate change awareness [1]. Over the course of their full lives, including production and use, EVs emit fewer emissions [2].

The popularity of EVs has accelerated technological development in the auto sector [3]. Subsidy plans based on the economic valuation of reduced greenhouse gas emissions have been suggested in order to encourage the purchase of BEVs [4]. Techniques for calculating a vehicle's life cycle and its environmental effect have been demonstrated and are used to analyze whether an EV can compete in a particular market and to pinpoint the key factors that affect an EV's viability [5]. The increasing use of EVs also makes it easier to incorporate renewable energy sources into the power grid. EVs can act as mobile energy storage units by being connected to the grid, facilitating energy transmission between the vehicle and the grid [6]. A more adaptable and sustainable energy system is facilitated by such integration, which also eases grid load [7].

In recent times, the EV range has been extended, and charging times have decreased due to more effective batteries and battery chargers [8,9]. The goal of continuing research in this field of EVs is to increase the capacity and longevity of energy storage systems. It also focuses on control strategies for battery management and wireless power transfer technologies [10,11]. Another research area in this field that holds great significance is efficient power conditioning systems. As EV technology advances, power electronics continue to

evolve to improve efficiency, reliability and performance [12]. Research focuses on developing semiconductor materials with improved efficiency, advanced control algorithms and innovative power conversion topologies to enhance the overall efficiency and capabilities of electric vehicles [13–18]. Research and development are focused on determining and analyzing dependable and effective power converter topologies [19].

DC–DC converters effectively transfer power between various voltage levels inside the vehicle by stepping the voltage up or down as necessary [20]. Based on whether galvanic isolation is offered or not, dc–dc converters are mainly categorized into two types: isolated and non-isolated [21]. Unlike isolated converters, which incorporate transformers to provide isolation, non-isolated converters are without transformers and are commonly used in various applications which do not require isolation or can be achieved using other means. According to this perspective, non-isolated dc–dc power converters are used for EVs over their bulkier and more expensive isolated equivalents [22]. The most common configurations in the non-isolated category are buck, boost, buck-boost, CUK, SEPIC, ZETA, positive output super-lift Luo and ultra-lift Luo [23–29].

Electric motors in EVs are powered by batteries using voltage source inverters. Maintaining the battery rated voltage at a relatively low level is useful for optimizing vehicle performance because it uses fewer series-connected cells. A higher number of parallel connected cell strings increases the redundancy of the backup system. Furthermore, it also helps to address the issues brought on by charge imbalance [30]. A high-voltage DC bus is required since the rated voltage and the output power of the motor are interdependent. Most models of electric cars that have entered the market in recent years are 400 V based. For instance, the Tesla Model 3 is built for 350 V dc link voltage and the Audi e-tron for 396 V [31,32]. However, Porsche was the first carmaker to design an EV with an 800 V powertrain when it introduced Taycan [33].

Figure 1 shows the power flow and the charging of the EV. Since the voltage level of the battery, grid and dc-link are different, battery–grid compatibility and battery-motor compatibility ought to be maintained. This necessitates the use of directional dc–dc converters in the vehicle to manage bidirectional power flow between battery and grid and also between battery and motor. The bidirectional feature in DC–DC converters pertains to their ability to transfer power in both directions, enabling power flow and voltage conversion in either direction between the input and output.

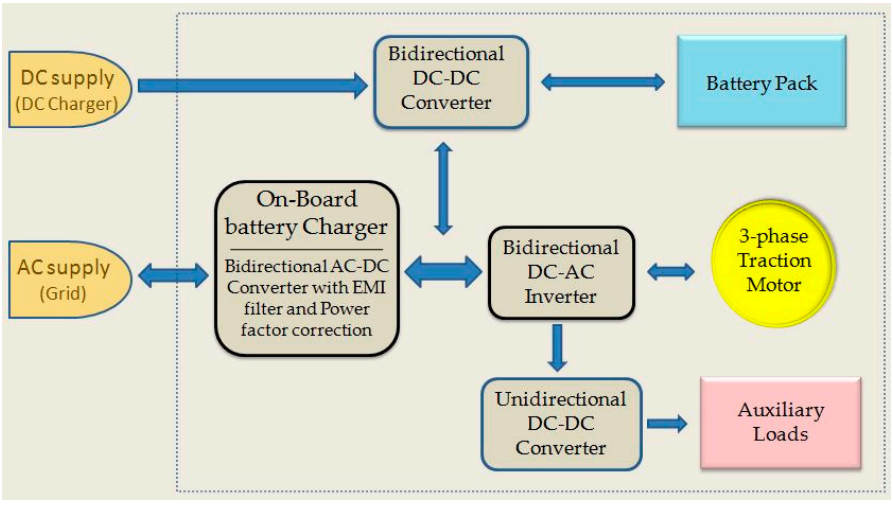

Figure 1. Charging and power flow in EV.

Bidirectional converters play a vital role in managing power flow, voltage regulation and energy optimization. The battery, which has a lower voltage, provides power to the higher-voltage-rated motor/inverter/dc link during normal vehicle operation. Consequently, the dc–dc converter serves as a boost converter. The buck action of the converter comes into play during the regenerative braking of the vehicle. Here, the power flows from

the traction motor, now behaving like a generator, to the battery [34]. Therefore, as seen in Figure 2, the bidirectional dc–dc converter will increase the voltage when power flows in one direction and decrease the voltage when power flows in the opposite direction. The arrows show the direction of power flow.

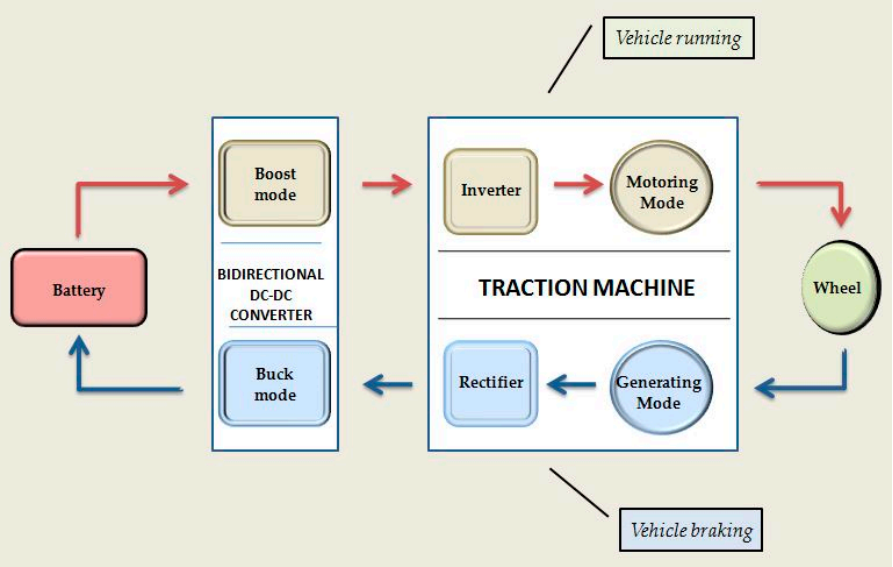

Figure 2. Power flow between battery and traction machine in EV.

The contributions of this research work are given below.

Conventional bidirectional half-bridge dc–dc converters with buck and boost modes have their own limitations [35]. Firstly, the achieved voltage gain does not allow precise speed control of the vehicle during running. Secondly, in order for the regenerative energy to be stored in the battery during the low-speed regenerative braking phase, the voltage generated by the traction machine must be increased. The objectives of this research are as follows:

- To propose a novel tri-mode non-isolated bidirectional dc–dc converter with three modes of operation: buck, boost and buck-boost;
- To develop a novel control strategy with pulse generation logic for all the switches;
- To introduce a mode transition algorithm for smooth changeover between modes.

The proposed converter operates as a boost converter during normal vehicle operation mode and gives double gain with a wide voltage range as compared to conventional bidirectional converter. As a result, the driver can obtain precise speed variation with the accelerator pedal, providing improved speed control. During regenerative braking, depending on the magnitude of voltage generated by the traction machine, the converter either works in the buck mode or the buck-boost mode depending on the control algorithm. If the generated voltage is more than double the voltage required for charging the battery, it works as buck converter giving half the gain at a broad voltage range compared to conventional buck converter. Else, the proposed converter operates in the buck-boost mode initiating its buck action should the voltage produced by the traction machine is more than the voltage required for charging the battery. If the generated voltage is less than what is required for charging the battery, the mode initiates its boost action. This usually happens at lower braking speeds and the converter boosts the voltage sufficiently to feed the regenerative energy to the battery. So during regenerative braking, both the buck and buck-boost modes are applicable. As energy is extracted even during low-speed regenerative braking, the efficiency of regenerative braking is enhanced. This research makes a significant contribution to the field of electric vehicles by enhancing regenerative braking efficiency and speed control.

This paper is organized as follows: Section 2 gives a review of the related research works. Section 3 presents the circuit configuration of the proposed converter and its operation and analysis for all the operating modes. Section 4 provides the design and the control strategy adopted along with the pulse generation logic for all the modes. It also gives the mode transition algorithm. Results are presented in Section 5 and the conclusion is given in Section 6.

2. Related Research Works

The development of non-isolated bidirectional converter with high gain, improved efficiency, and high-power density is the current area of research emphasis. It is anticipated to be smaller and lighter. Meanwhile, gain and efficiency must be preserved over a broad working load range. R. J. Wai et al. [36] proposed a coupled inductor-based dc–dc bidirectional converter with three power switches to accomplish soft switching, voltage clamping, and a good voltage conversion ratio. Y P Hsieh et al. [37] designed a coupled inductor-based bidirectional dc–dc converter with a low component count in which two capacitors are charged in parallel and discharged in series with the linked inductor. A variable inductor in the bidirectional converter presented in [38] allows it to accommodate a variety of changes in load.

To produce high step up/down voltage gain, coupled inductors and voltage multiplier cells are occasionally combined [39]. Y. Zhang et al. introduced coupled inductor with adjustable turns ratio to give a wide voltage-gain range [40]. Recently, Malik et al. designed the bidirectional converter using coupled inductor to achieve all the mentioned features using lower number of components. The volume and cost of the said converter is significantly lower achieving a high efficiency [41].

Bidirectional dc–dc converters based on switching capacitors provide an effective means of moving energy back and forth between DC sources. Although they require careful consideration in both their design and control, they offer great response times and efficiency [42–44]. A switched-capacitor bidirectional dc–dc converter with a high step-up/step-down voltage gain is proposed for use in electric vehicles equipped with hybrid energy systems. The benefits of the converter include a common ground, a limited number of components, a simple circuit, and a wide voltage-gain range [45]. A bidirectional switched-capacitor/switched-quasi-Z-source hybrid dc–dc converter with a broad voltage gain range is presented by same researcher. The benefits of wide voltage gain range and lower voltage stress on the power switches are achieved [46]. Y Zhang et al. [47] introduced a novel bidirectional converter that employs a switched capacitor interleaved configuration, integrating the three-phase interleaved structure with switched capacitor cells. Sometimes, researchers have combined the switched inductor and switched capacitor techniques to achieve a broad voltage gain range along with reduced voltage stress on power switches [48].

To increase the voltage gain and efficiency, [49] introduced bidirectional converter that has two boost converters with four power switches a capacitor and two inductors. N Elsayad et al. [50] designed a new bidirectional switched-capacitor and quadratic-based dc–dc converter. A unique non isolated bidirectional dc–dc converter composed of a quadratic voltage cell, a switched-capacitor cell, and a zero-current ripple cell was developed [51]. T. Sojoudi et al. [52] proposed similar topology with fewer switches using Input–Output Feedback Linearization (IOFL) controller to obtain the same benefits as in [51]. Interleaved structures have the advantages of distribution of energy through multiple phases, enhancing overall performance, decrease in voltage stress across switches and current ripples [53,54]. V. Rathore et al. [55] proposed the topology structure which converts two split capacitor half-bridge circuits into series and parallel by symmetrically modulating a bidirectional two quadrant switch. In the same lines, R. R. De Melo et al. [56] provides an interleaved architecture which is a good option for high power, high current levels with minimum number of components and a higher efficiency over a broad load range.

A study carried out by Tine Konjedic et al. [57] examines a control strategy for synchronous rectification-based conventional non-isolated bidirectional dc–dc converters that uses the entire operating range to reliably achieve zero-voltage switching transitions. J Chen et al. [58] carried out research work and developed a multistage non-isolated bidirectional high-voltage conversion ratio converter. The converter uses just n+2 switches and is n times more efficient than a traditional buck/boost converter.

Switching losses in conventional DC–DC converters can be rather large, especially at high frequencies or high load currents. By guaranteeing that the switching transitions take place while the voltage or current across the switching devices is nearly zero, soft switching approaches work to lessen these losses and improve efficiency [59,60]. To decrease current ripple and switching loss and considerably improve converter efficiency and power density, a multiphase quasi-resonant zero-current switching (ZCS) switched capacitor bidirectional dc–dc converter construction is presented [61]. L Jiang et al. [62] presents the auxiliary circuit comprising of switches, diodes, coupled inductor and an independent inductor and applies it to half-bridge configuration. The proposed converter in [63] uses four switches alongside an inductor and capacitor and can turn on all switches with zero voltage and turn off some switches with zero current in continuous conduction mode in both forward and reverse modes. J.W. yang et al. [64] developed a high-efficiency bidirectional dc–dc converter that exhibits ZVS over the full range of loads and low circulating current. Once more, they introduced a converter that uses an active snubber made up of auxiliary switches, diodes, an inductor, and a capacitor to accomplish ZVS of main switches [65].

M Aamir et al. [66] proposed circuit with a voltage clamping network along with three active switches and a coupled inductor to obtain ZVS. In order to provide soft switching in all four switches in both buck and boost operation modes, S. Dusmez et al. [67] merged two identical zero-voltage transition (ZVT) cells with the traditional three level topology. This made it possible to operate with a higher switching frequency and achieve a better power density and improve efficiency. To provide ZVS, a reduced component bidirectional converter with an auxiliary resonant network is introduced [68]. N. Molavi et al. [69] introduced a bidirectional DC–DC converter with soft switching, high-voltage conversion ratio, and low-voltage stress across semiconductor devices. Additionally, zero-current switching performance totally resolves the body diode reverse recovery issue.

R.H. Ashique et al. [70] proposed converter with high gain in the continuous current mode by using energy storage element in between. Soft-switching conditions for both switches are also provided by maintaining a recycling current in the auxiliary circuit made up of a small inductor and two capacitors [71].

The literature review shows that bidirectional converter research is focused on improving efficiency, power density, and voltage conversion ratios. Various approaches, such as coupled inductors, switching capacitors and interleaved structures have been explored. These designs aim to reduce voltage stress across switches, minimize current ripple and achieve soft switching, ultimately improving efficiency and power density. Researchers have also combined multiple techniques, like coupled inductors and switching capacitors, to achieve a wide voltage gain range and efficient power transfer. Different control strategies, including synchronous rectification, have been employed to further enhance performance. The proposed novel converter configuration provides the wide voltage gain necessary and more recovery of regenerative braking energy.

3. Configuration and Operation

The circuit configuration of the proposed converter and its operation in all the three modes is described in this section.

3.1. Configuration of the Proposed Converter

The proposed non-isolated bidirectional converter, as shown in Figure 3, consists of six switches (S_1–S_6), an inductor (L), capacitances (C_{H1} and C_{H2}) on the high-voltage side and capacitance (C_L) on the low-voltage side. As a modification of the conventional

bidirectional buck and boost converter, it uses two sections of the same. Also two additional switches one in series and one in shunt are used. V_b is the battery voltage and V_d is the dc link voltage. V_b' is the output voltage of the converter when it operates in the buck or buck-boost mode during regenerative braking. So this is the voltage available at the terminals of the battery for charging it during regenerative braking.

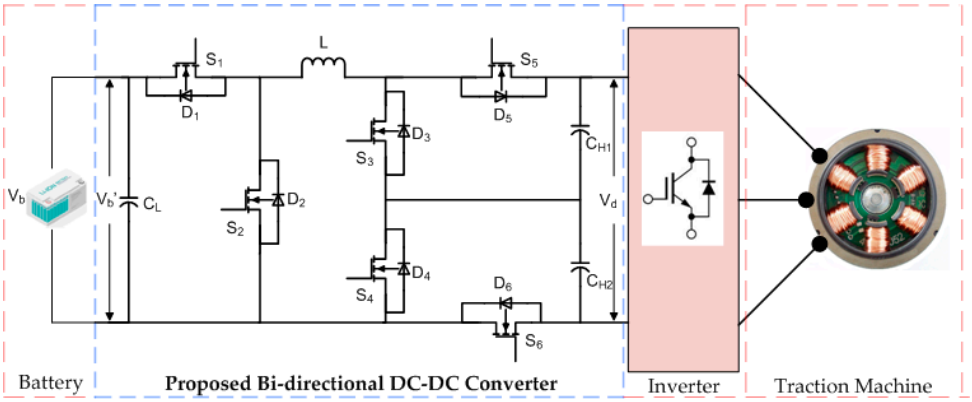

Figure 3. Proposed non-isolated bidirectional dc–dc converter.

In normal vehicle operation (boost mode), switch S_1 is always ON and S_2 is OFF. Switches S_3 and S_4 are controlled using PWM techniques. During regenerative braking, when the converter operates in the buck mode, again switch S_1 is always ON and S_2 is OFF but switches S_5 and S_6 are controlled for their duty cycles. The buck-boost mode of regenerative braking utilizes switches S_2, S_5 and S_6 for PWM control. There are four operational intervals for all the modes of operation. The following assumptions are made for carrying out the analysis: (i) ON-state resistance of the MOSFETs and ESR of capacitors are not taken into account. (ii) The voltage across the capacitors C_{H1}, C_{H2}, and C_L is constant as they are sufficiently large capacitors C_{H1}, C_{H2}, and C_L are large enough, and the voltages across the capacitors can be treated as constant. (iii) The capacitors C_{H1} and C_{H2} have the same capacitance; hence, the voltage across each of them is $V_d/2$.

3.2. Operation and Analysis

This sub-section gives the detailed circuit operation for the boost, buck and buck-boost modes. Circuit analysis for every interval of the mode based on the theoretical waveforms with PWM switching is presented.

3.2.1. The Boost Mode

This mode corresponds to the normal running of the electric vehicle. i_d is the dc link current. V_L is the voltage across the inductor. The equivalent circuit is shown in Figure 4. V_{s1} to V_{s6} and i_{s1} to i_{s6} are the voltages and currents for the respective switches S_1 to S_6. R_d is the dc link resistance for boost equivalent circuit. i_{CH1}, i_{CH2} and$V_{d1,}$ V_{d2} are the currents and voltages through the dc link capacitances C_{H1} and C_{H2}. For this mode, switch S_1 is ON and S_2 is OFF. T_p is the switching time period and δ is the duty cycle factor for the MOSFETs. V_{g1} to V_{g6} are the gate pulses for the MOSFETs.

(a) Interval-I (t_0–t_1): Switches S_5 and S_6 are OFF. Switches S_3 and S_4 are turned ON. As seen in Figure 5a, the current flows from the battery to the inductor L through switch S_1 and back to the battery through switches S_3 and S_4. L receives energy from the battery at voltage V_b and the current through it rises as seen in the theoretical waveforms depicted in Figure 6. C_{H1} and C_{H2} provide energy to the dc link to maintain voltage V_d.

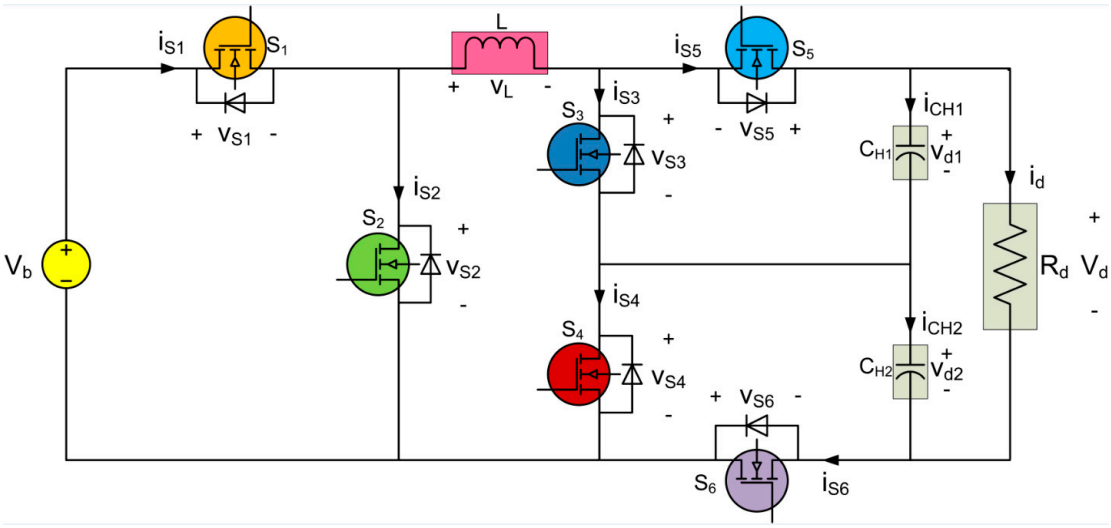

Figure 4. Equivalent circuit in the boost mode. Color indicates the circuit component.

Therefore, the voltage across L is given by Equation (1),

$$V_L = V_b \tag{1}$$

The current through L as shown by Equation (2) is,

$$i_L(t) = i_L(t_0) + \frac{V_b}{L}(t - t_0) \tag{2}$$

(b) Interval-II (t_1–t_2): At t_1, Switch S_3 is turned OFF and S_5 turned ON. The current now flows from the battery and inductor to the dc link and capacitor C_{H1} through the switches S_1, S_5 and S_4 as shown in Figure 5b.The inductor and battery provide energy to the dc link. C_{H1} is also charged with this energy. Current flow through L decreases and its polarity is reversed as shown. C_{H1} and C_{H2} maintain the dc link voltage V_d. Switch S_5 is employed as synchronous rectifier.

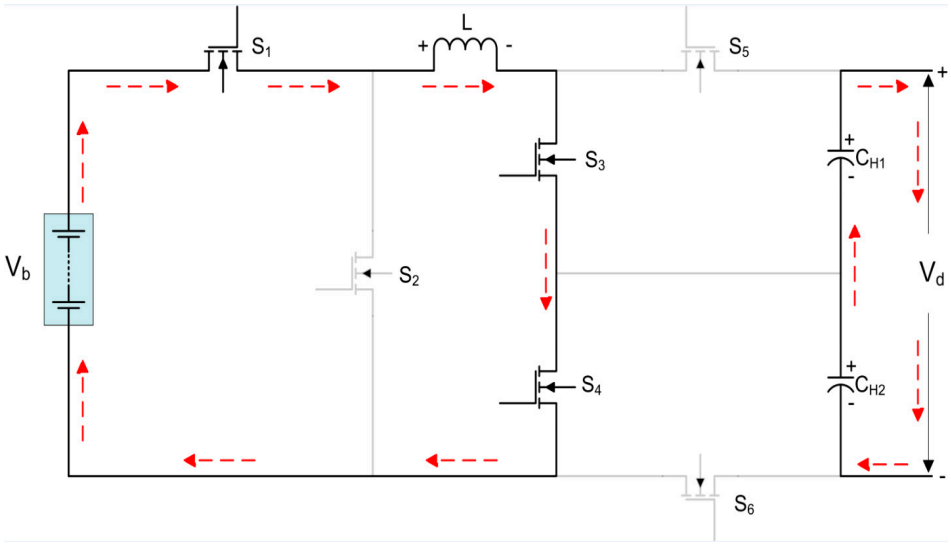

(**a**)

Figure 5. *Cont.*

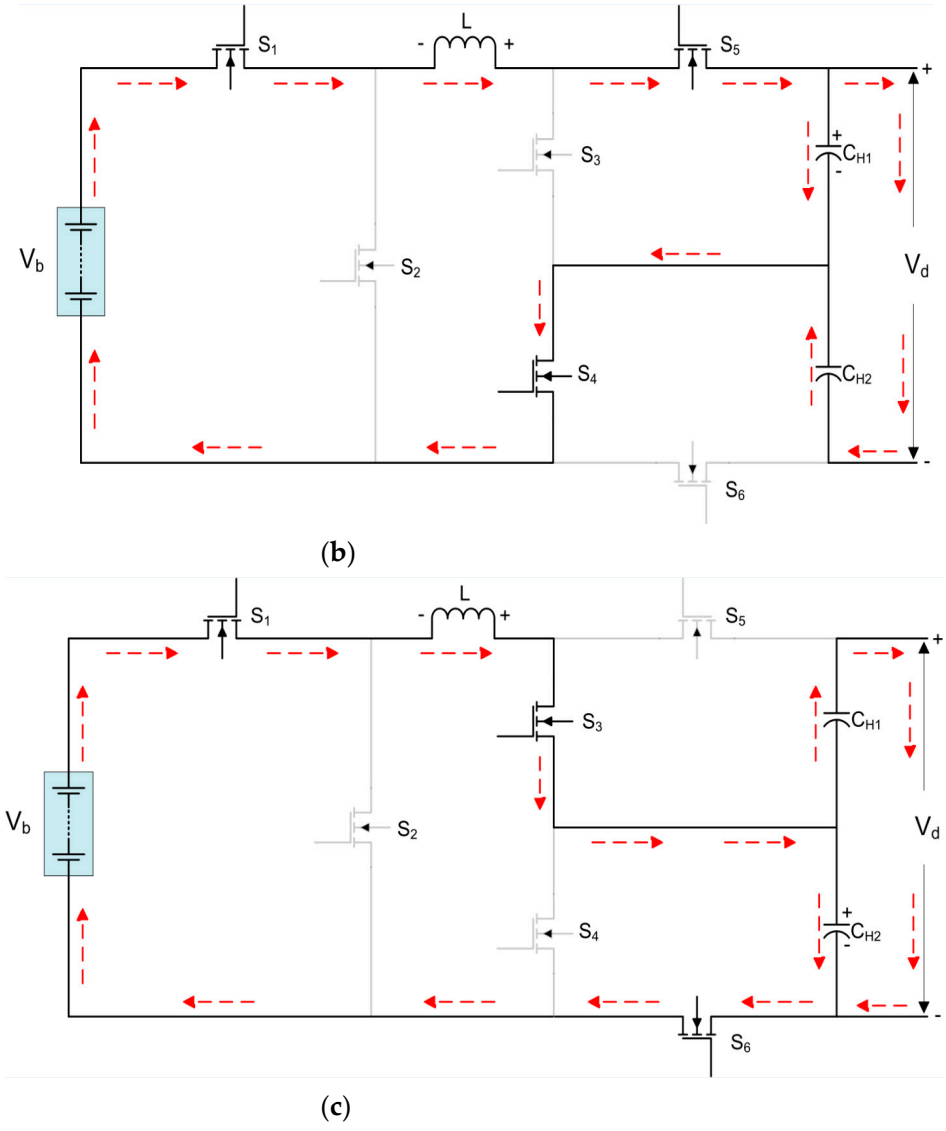

Figure 5. Operation of the proposed converter in the boost mode. (**a**) Interval-I (t_0–t_1) and Interval-III (t_2–t_3); (**b**) Interval-II (t_1–t_2); (**c**) Interval-IV (t_3–t_4). Red arrow indicates current flow direction.

Synchronous rectification is a technique in which the rectification diode of in the converter is replaced by active switch in order to improve efficiency. Diodes have inherent voltage drop and large reverse recovery loss leading to reduced efficiency. In synchronous rectification, the switches are turned on and off in synchronization with the input voltage, thereby actively directing the current flow in the circuit. This active control allows faster switching times and improves the dynamic performance of the converter [72]. The switch which performs the role of the diode is called the synchronous rectifier for that interval. Equations (3) and (4) represent the voltage and current equations for this interval.

$$\begin{aligned} -V_L &= \frac{V_d}{2} - V_b \\ V_L &= V_b - \frac{V_d}{2} \end{aligned} \tag{3}$$

$$i_L(t) = i_L(t_1) + \frac{1}{L}\left(V_b - \frac{V_d}{2}\right)(t - t_1) \tag{4}$$

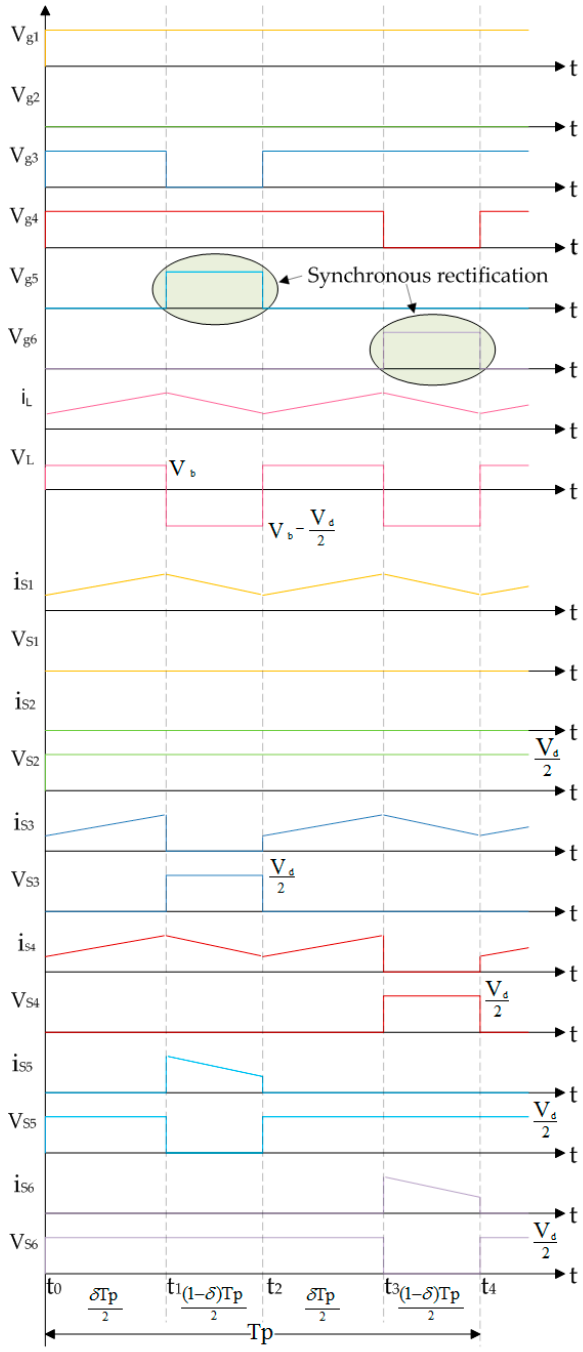

Figure 6. Theoretical waveforms with PWM switching for the boost mode.

(c) Interval-III (t_2–t_3):Switch S_5 is turned OFF and S_3 is turned ON at instant t_2. Similar to interval I, this interval sees an increase in current flowing through L and the transfer of energy from the battery. Polarity across L changes once more. C_{H1} and C_{H2} discharge energy to the dc link as depicted in Figure 5a. So the inductor voltage and current are shown in Equations (5) and (6).

$$V_L = V_b \tag{5}$$

$$i_L(t) = i_L(t_2) + \frac{V_b}{L}(t - t_2) \tag{6}$$

(d) Interval-IV (t_3–t_4): At instant t_3, the switch S_4 is turned OFF and S_6 is turned ON.As seen in Figure 5c, the current is now flowing from the battery and inductor to the dc link and capacitor C_{H2} through the switches S_1, S_3, and S_6. The DC link is powered by the inductor and battery. This energy is also charged in C_{H2}. As shown, the polarity of L is inverted and its current flow decreases. DC link voltage V_d is maintained by C_{H1} and C_{H2}. Switch S_6 performs the role of synchronous rectifier.

The voltage across L is given by Equation (7),

$$V_L = V_b - \frac{V_d}{2} \tag{7}$$

Also current through L as given by Equation (8) is,

$$i_L(t) = i_L(t_3) + \frac{1}{L}\left(V_b - \frac{V_d}{2}\right)(t - t_3) \tag{8}$$

The average value of the voltage applied across an ideal inductor winding must be zero, according to the inductor volt-second balance principle [73].

Therefore, considering the four intervals Equation (9) is formulated,

$$\left[\int_0^{\delta\frac{T_p}{2}} V_L dt\right] + \left[\int_0^{(1-\delta)\frac{T_p}{2}} V_L dt\right] + \left[\int_0^{\delta\frac{T_p}{2}} V_L dt\right] + \left[\int_0^{(1-\delta)\frac{T_p}{2}} V_L dt\right] \tag{9}$$

Substituting Equations (1), (3), (5) and (7) in Equation (9),

Equation (10) gives the voltage gain of the proposed converter. As seen, it is double as compared to the conventional converter.

$$\frac{V_d}{V_b} = \frac{2}{1-\delta} \tag{10}$$

3.2.2. The Buck Mode

This mode corresponds to the regenerative braking of the electric vehicle. The equivalent circuit and circuit operation for the buck mode are shown in Figures 7 and 8, respectively. R_b is the output resistance as seen when the proposed converter operates in the buck mode. For this mode, switch S_1 is ON and S_2 is OFF. The theoretical waveforms with PWM switching for this mode are shown in Figure 9.

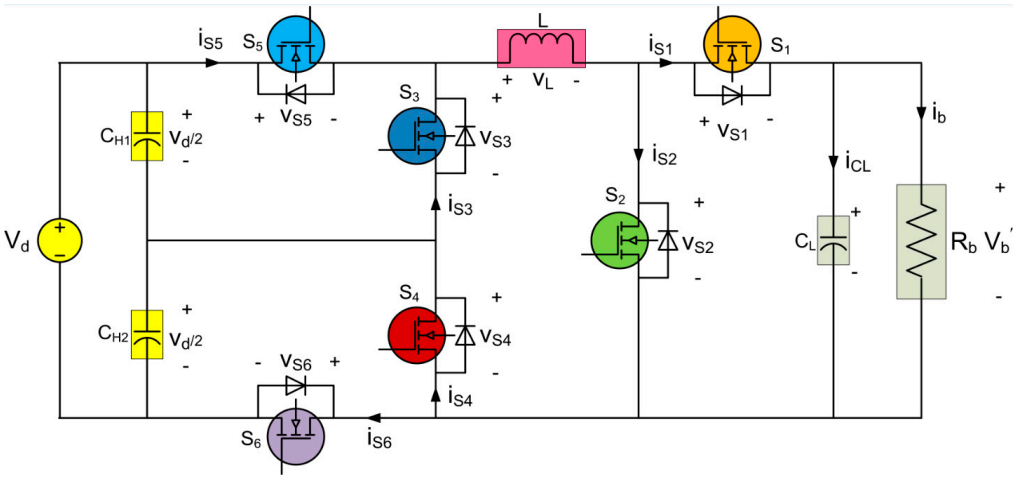

Figure 7. Equivalent circuit in the buck mode and the buck-boost mode. Color indicates the Circuit component.

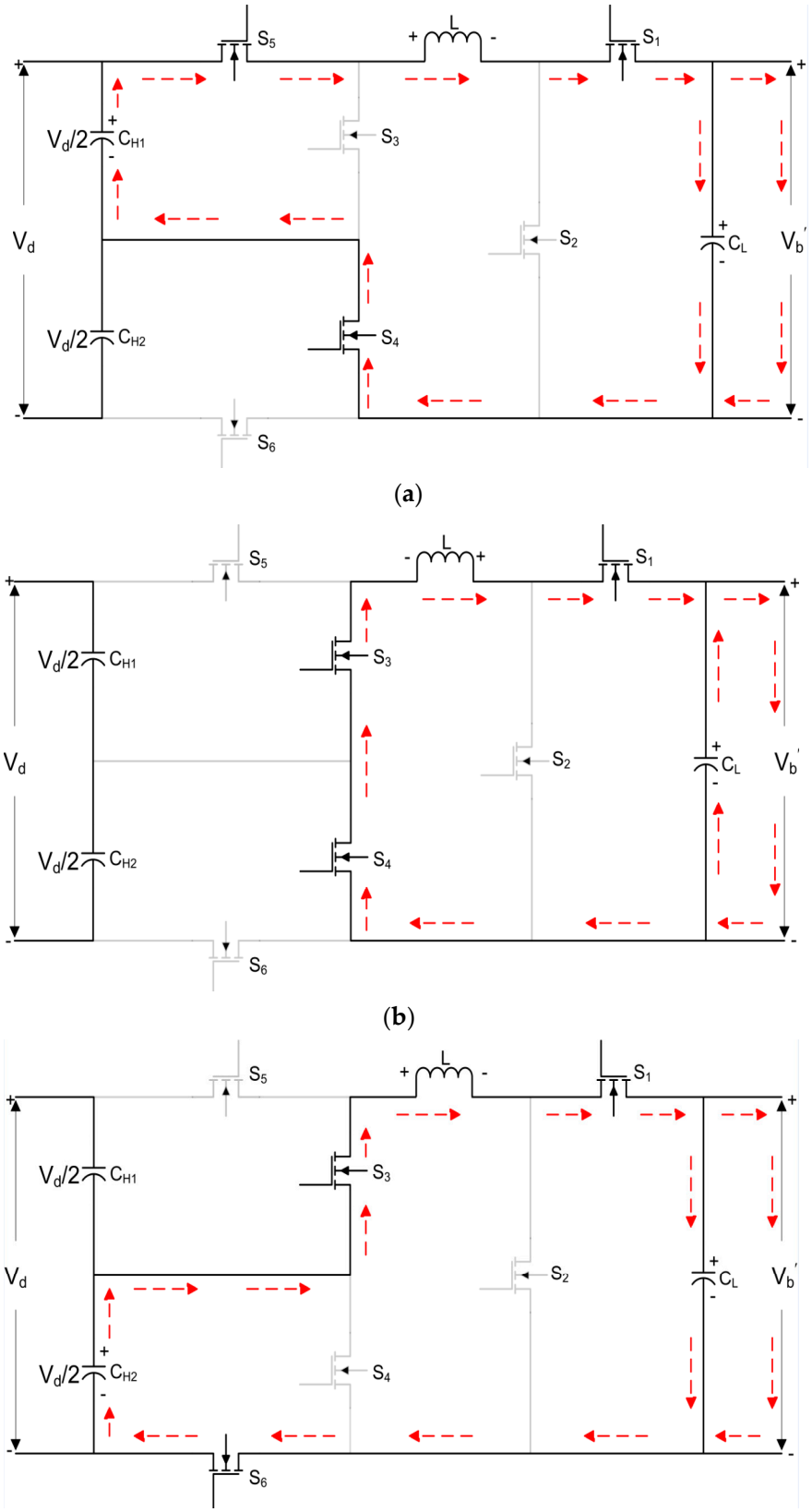

Figure 8. Operation of the proposed converter in the buck mode: (**a**) Interval-I (t_0–t_1); (**b**) Interval-II (t_1–t_2) and Interval-IV (t_3–t_4); (**c**) Interval-III (t_2–t_3). Red arrow indicates current flow direction.

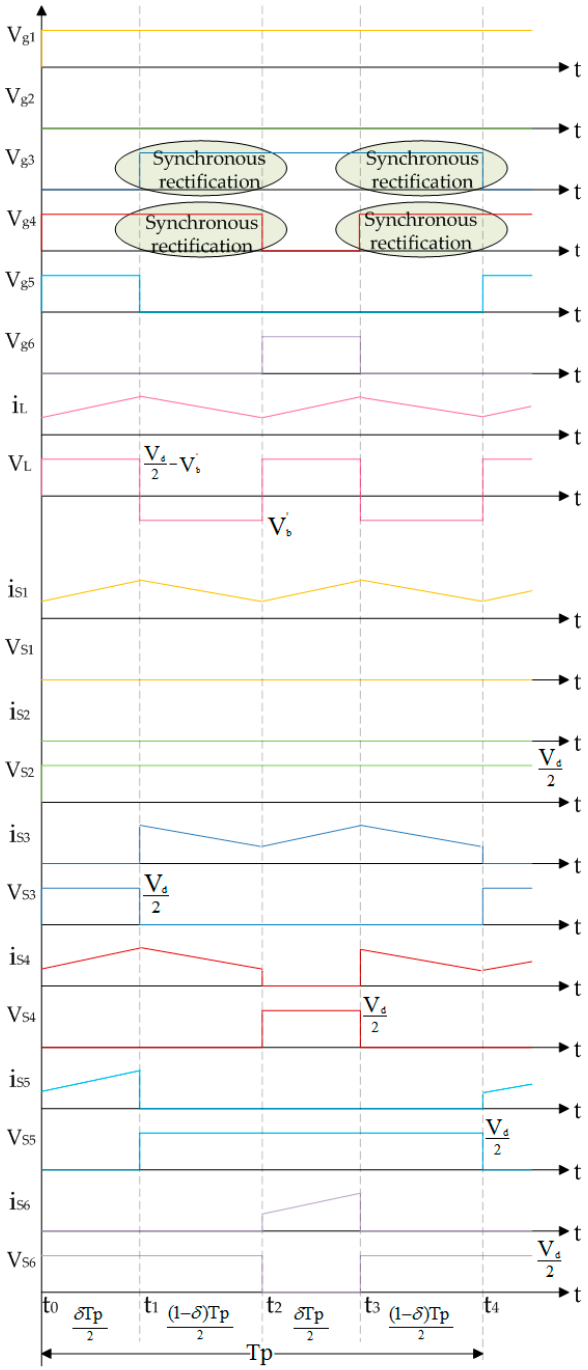

Figure 9. Theoretical waveforms with PWM switching for the buck mode.

(a) Interval-I (t_0–t_1):Both the switches S_3 and S_6 are OFF. S_4 and S_5 are switched ON at t_0. The current flows from the dc link capacitance C_{H1} to the inductor L through switch S_5 and then to the output capacitance C_L/battery through switch S_1 and back to the dc link through switch S_4 as indicated in Figure 8a. L receives energy from the dc link and current through it rises. Also, C_L is charged by this energy. This energy comes from the regenerative braking of the vehicle.

Therefore, Equation (11) gives voltage across L,

$$V_L = \frac{V_d}{2} - V'_b \quad (11)$$

The current through L is given by Equation (12),

$$i_L(t) = i_L(t_0) + \frac{1}{L}\left(\frac{V_d}{2} - V_b'\right)(t - t_0) \tag{12}$$

(b) Interval-II (t_1–t_2): Now, switch S_5 is turned OFF and S_3 turned ON. Through switches S_1, S_4, and S_3, energy stored in the inductor L is transmitted to the battery. During this time, the current is allowed to freewheel through the synchronous rectifiers S_3 and S_4. As shown in Figure 8b, the polarity of L is reversed as the magnitude of current flow through it decreases. C_L also transfers its stored energy to the battery.

The voltage across L is given by Equation (13),

$$\begin{aligned} -V_L &= V_b' \\ V_L &= -V_b' \end{aligned} \tag{13}$$

Equation (14) gives current through L,

$$i_L(t) = i_L(t_1) - \frac{V_b'}{L}(t - t_1) \tag{14}$$

(c) Interval-III (t_2–t_3):This interval starts with the turning OFF of switch S_4 and turning ON of switch S_6.As shown in Figure 8c, the current flows from the dc link capacitance C_{H2} to the inductor L via switch S_3, to the output capacitance C_L/battery through switch S_1, and back to the dc link via switch S_6. The dc link provides energy to L, which causes a rise in current flow. This energy charges C_L as well. The vehicle's regenerative braking is where this energy is generated. So the inductor voltage and current are as given by Equations (15) and (16).

$$V_L = \frac{V_d}{2} - V_b' \tag{15}$$

$$i_L(t) = i_L(t_2) + \frac{1}{L}\left(\frac{V_d}{2} - V_b'\right)(t - t_2) \tag{16}$$

(d) Interval-IV (t_3–t_4): Switch S_6 is turned OFF and S_4 turned ON. During this interval, the current freewheels through switches S_1, S_4, and S_3, to transfer the energy stored in the inductor to the battery. This is shown in Figure 8b. S_3 and S_4 operate as synchronous rectifiers. Current flow through L decreases and its polarity is inversed.

The inductor voltage is shown by Equation (17).

$$V_L = -V_b' \tag{17}$$

The current is given by Equation (18),

$$i_L(t) = i_L(t_3) - \frac{V_b'}{2}(t - t_3) \tag{18}$$

Applying the volt-second balance principle to the inductor taking into consideration the four intervals, Equation (19) is formulated [73].

$$\left[\int_0^{\delta\frac{T_p}{2}} V_L dt\right] + \left[\int_0^{(1-\delta)\frac{T_p}{2}} V_L dt\right] + \left[\int_0^{\delta\frac{T_p}{2}} V_L dt\right] + \left[\int_0^{(1-\delta)\frac{T_p}{2}} V_L dt\right] \tag{19}$$

Substituting Equations (11), (13), (15) and (17) in Equation (19),

Equation (20) gives the voltage gain of the proposed converter in the buck mode. It is half as compared to the conventional converter.

$$\frac{V_b'}{V_d} = \frac{\delta}{2} \tag{20}$$

3.2.3. The Buck-Boost Mode

This mode is used during the regenerative braking of the electric to buck or to boost the regenerated voltage. Figures 7 and 10, respectively, depict the corresponding equivalent circuit and circuit operation for this mode. The theoretical waveforms are presented in Figure 11.

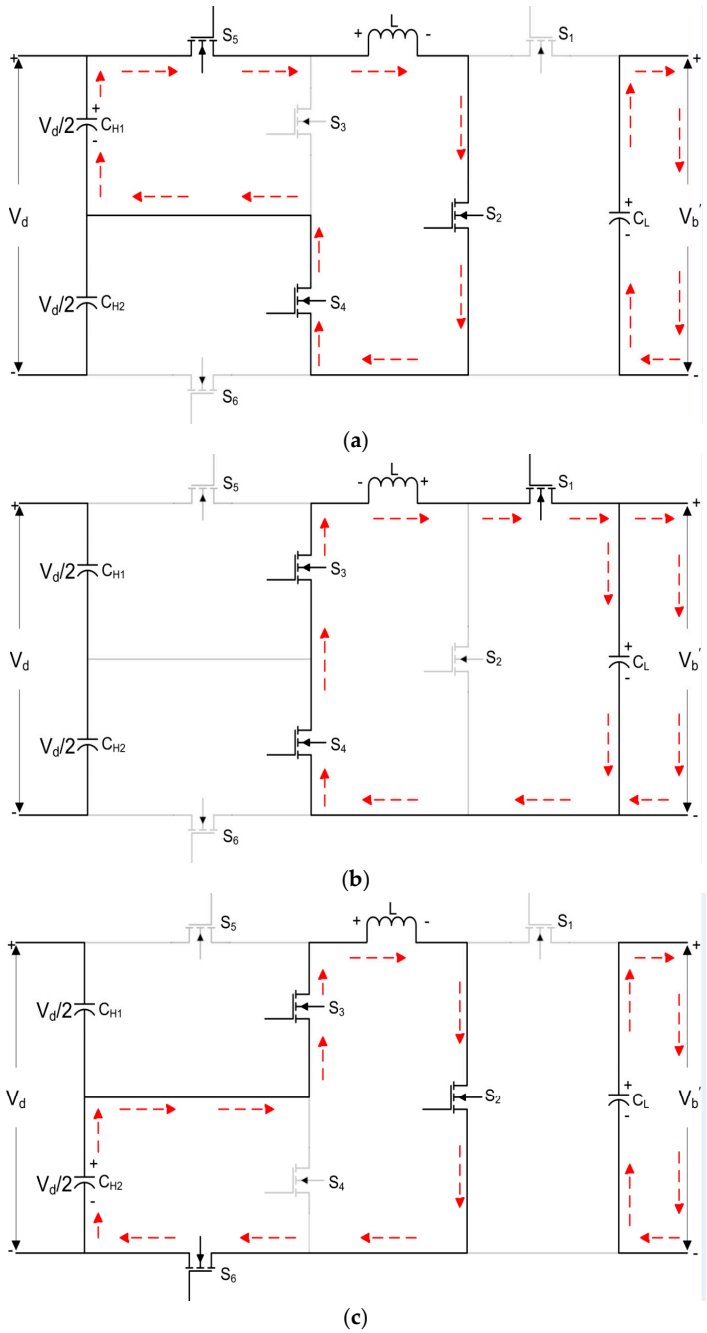

Figure 10. Operation of the proposed converter in the buck-boost mode: (**a**) Interval-I (t_0–t_1); (**b**) Interval-II (t_1–t_2) and Interval-IV (t_3–t_4); (**c**) Interval-III (t_2–t_3). Red arrow indicates current flow direction.

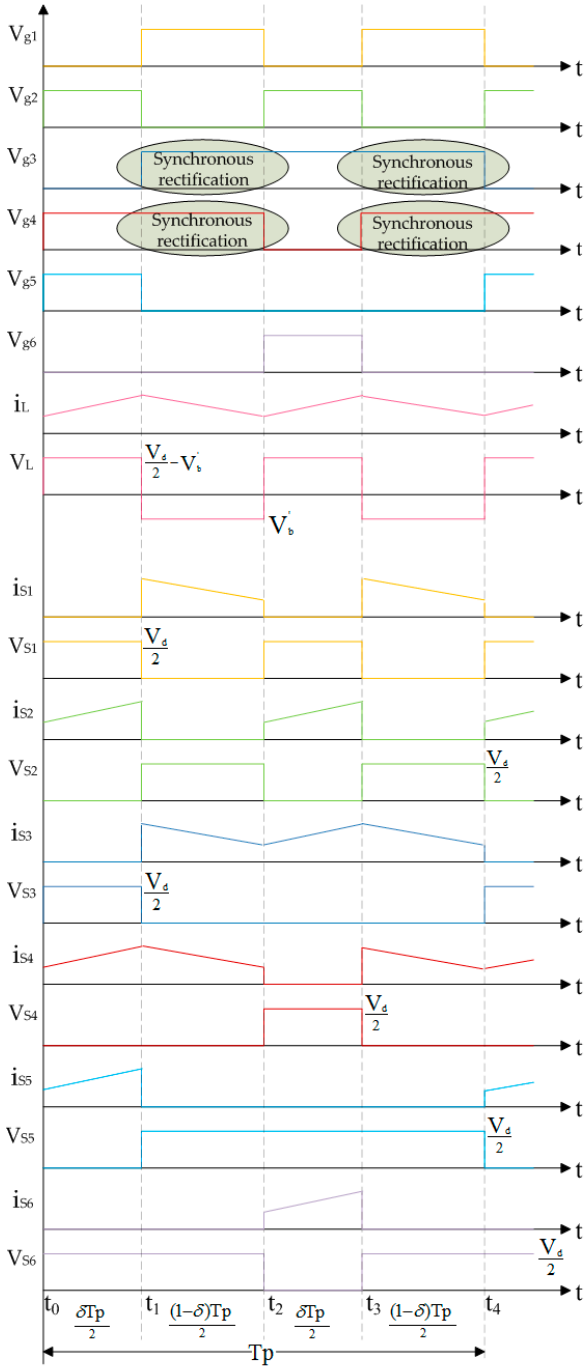

Figure 11. Theoretical waveforms with PWM switching for the buck-boost mode.

(a) Interval-I (t_0–t_1):The switches S_1, S_3 and S_6 are OFF and S_2,S_4 and S_5 are turned ON. The current flows from the dc link capacitance C_{H1} to the inductor L through switch S_5 and then back to the dc link through switch S_2 and S_4 as shown in Figure 10a. L is energized by the dc link, and the current via it increases. The inductor polarity is indicated as such. C_L releases the energy it has stored into the battery. The voltage across L is given by Equation (21).

$$V_L = \frac{V_d}{2} \tag{21}$$

Current, as given by Equation (22) is

$$i_L = i_L(t_0) + \frac{1}{L}\left(\frac{V_d}{2}\right)(t - t_0) \tag{22}$$

(b) Interval-II (t_1–t_2):This interval starts with switches S_2 and S_5 being turned OFF. At the same time switches S_1 and S_3 are turned ON. The source that is the dc link is cut off by switch S_5 and the energy stored in the inductor during interval-I, charges the battery and the capacitor C_L. Inductor L experiences a drop in current and a polarity change. The current flow direction during this interval is shown in Figure 10b. S_3 and S_4performthe role of synchronous rectifiers.

The voltage across L is given by Equation (23),

$$\begin{aligned} -V_L &= V_b' \\ V_L &= -V_b' \end{aligned} \tag{23}$$

Equation (24) gives current through L.

$$i_L(t) = i_L(t_1) - \frac{V_b'}{L}(t - t_1) \tag{24}$$

(c) Interval-III (t_2–t_3): Switches S_1 and S_4 are currently turned OFF. S_2 and S_6 switches are turned on. As depicted in Figure 10c, the current flows from the dc link capacitance C_{H2} to the inductor L via switch S_3, and then it returns through switches S_2 and S_6 to the dc link. In the process, L stores energy from the dc link, as current through it increases. The inductor has the indicated polarity. The battery receives the energy that C_L held during the prior interval. So Equations (25) and (26) gives voltage and current through the inductor respectively.

$$V_L = \frac{V_d}{2} \tag{25}$$

$$i_L(t) = i_L(t_2) - \frac{V_d}{L}(t - t_2) \tag{26}$$

(d) Interval-IV (t_3–t_4):Switch S_2 and S_6 are turned OFF to start this interval. This is accompanied by the turn ON of switches S_1 and S_4. Figure 10b indicates this switching. This interval is similar to interval-II, and the battery and capacitor C_L are charged by the energy stored in the inductor.

The voltage across L is given by Equation (27) as,

$$\begin{aligned} -V_L &= V_b' \\ V_L &= -V_b' \end{aligned} \tag{27}$$

The current through L is indicated by Equation (28),

$$i_L(t) = i_L(t_3) - \frac{V_b'}{L}(t - t_3) \tag{28}$$

Utilizing the volt-second balancing concept to the inductor while taking the four intervals into account, Equation (29) is formulated [73],

$$\left[\int_0^{\delta\frac{T_p}{2}} V_L dt\right] + \left[\int_0^{(1-\delta)\frac{T_p}{2}} V_L dt\right] + \left[\int_0^{\delta\frac{T_p}{2}} V_L dt\right] + \left[\int_0^{(1-\delta)\frac{T_p}{2}} V_L dt\right] \tag{29}$$

Substituting Equations (21), (23), (25) and (27) in Equation (29),

Equation (30) gives the voltage gain of the proposed converter in the buck-boost mode. It is half as compared to the conventional buck-boost converter.

$$\frac{V_b'}{V_d} = \frac{\delta}{2(1-\delta)} \tag{30}$$

4. Design and Control Strategy

The circuit parameter design based on the specifications considered is provided in this section. Also the control strategy applied is explained. A mode transition algorithm to change the pulse pattern during mode switching is given.

4.1. Design of the Proposed Converter

The proposed converter is designed considering the specifications as listed in Table 1. The power level corresponds to the power rating of the traction machine. The dc link voltage is the motor voltage if it is DC or it is the inverter input voltage if the motor is AC. This is the high-voltage side of the converter. The lithium-ion battery is rated for 48 V, with the voltage range mentioned in the bracket corresponding to the battery charge condition from discharged to fully charged condition. The voltage range 56–56.8 V is the voltage required for charging the battery. This should be the converter output voltage in the buck and buck-boost modes which corresponds to the regenerative braking.

Table 1. Design specifications for the proposed converter.

Design Specifications	Notation	Values
Power level	P	1500 W
DC link voltage (High side)	V_d	300 V
Battery voltage (Low side)	V_b	48 V (41–54.6 V)
Converter output voltage-buck and buck-boost mode (Low side)	V_b'	56 V (56–56.8 V)
Switching frequency	f_s	100 kHz
Main inductor	L	110 µH
Low-side capacitor	C_L	100 µF
High-side capacitors	C_{H1} and C_{H2}	100 µF

The switching frequency is set to 100 kHz and the inductor and capacitor values are calculated for the given specifications [74]. The inductor value is selected optimally to take care of all the three modes.

Critical value of inductance is given by Equation (31),

$$L_C = \frac{V_b(V_d - V_b)}{\Delta I_b \cdot f_s \cdot V_d} \tag{31}$$

ΔI_b is the ripple current of inductor and is considered to be 15% of the input current.

The calculated value of critical inductance is 86 µH. Since continuous conduction mode is considered, the selected value of inductance is higher than the critical value.

Similarly, critical value of capacitance as given by Equation (32) is,

$$C_C = \frac{\Delta I_b}{8 \cdot f_s \cdot \Delta V_o} \tag{32}$$

ΔV_o is the ripple value of output voltage and is assumed to be 0.1% of the output voltage. The critical value of capacitance is calculated as 26 µF. The selected value is higher than the critical value. The selected values are tabulated in Table 1.

4.2. Control Strategy

The closed loop controller and the pulse generation logic for all the three operating modes of the proposed converter are presented in this section.

4.2.1. Closed Loop Controller

The control strategy for the proposed bidirectional converter is shown in Figure 12. Depending on the current working mode, the converter's input and output voltages are V_b or V_d and V_d or V_b', respectively. The single accelerator/brake pedal decides the normal drive operation or the braking operation depending on whether the pedal is engaged or released.

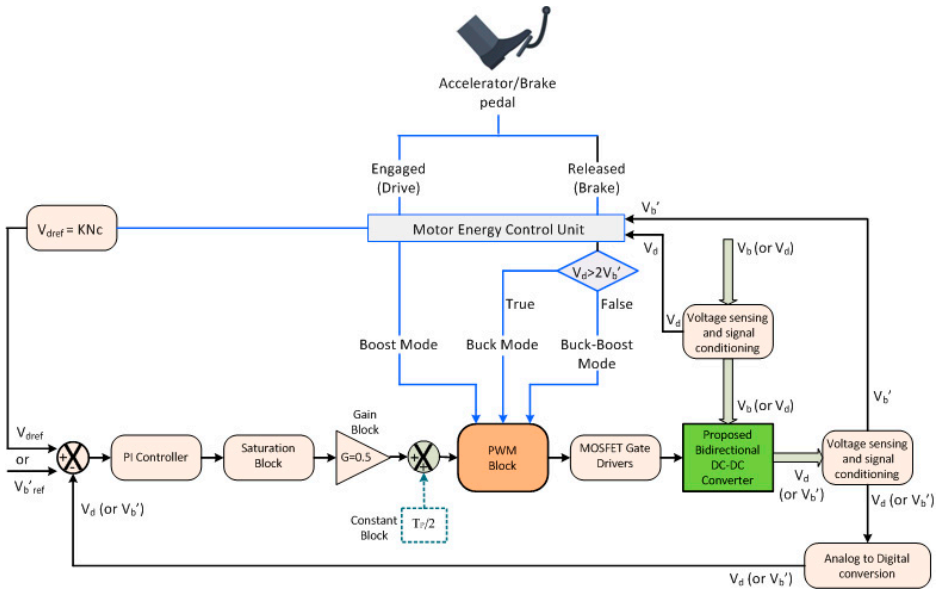

Figure 12. Control strategy for the proposed converter.

During normal vehicle driving operation (boost mode), the reference voltage V_{dref} is varied depending upon the motor speed expected. V_{dref} is calculated by the reference voltage calculation block from speed command N_c based on the accelerator/brake pedal and the proportionality constant K. The output voltage V_d is sensed, conditioned and then compared with the reference voltage. Accordingly, the duty cycle is estimated by the PWM block and pulses are generated for the corresponding MOSFETs to attain the intended output voltage in order to attain the required speed. The motor energy control unit controls these actions.

Regenerative braking corresponds to the buck and buck-boost modes of the converter. The voltage generated by the traction machine during regenerative braking varies depending upon the speed of the machine at that instant. The generated voltage (dc link voltage) is now the input to the converter. If the generated voltage is greater than V_b', the converter needs to lower the voltage to V_b'. As mentioned earlier, V_b' is the voltage required to charge the battery. But if the generated voltage is less than V_b', it has to boost it to give the required voltage V_b' to charge the battery. From Equations (20) and (30), it is clear that the proposed converter has to work in the buck mode only if the generated voltage V_d is greater than $2V_b'$ to reduce the voltage. Else it has to operate in the buck-boost mode to increase the voltage. $V_b'_{ref}$ is kept constant.

The transfer functions derived from the converter modeling and motor modeling equations are used to design the proportional–integral (PI) controller. The Ziegler Nichols technique is used to tune the controller, and the values for Kp and Ki (proportional and integral constants) are determined as 58.55×10^{-3} and 0.718, respectively [75]. Due to the fact that the duty cycle is half that of a conventional converter, the gain block with 0.5 gain is introduced. The major switches (S_3 and S_4) executing the boost action must run for an

additional amount of time during the boost mode that is equal to half the switching time period $T_p/2$ above the duty time. As a result, the constant block with $T_p/2$ is merely added to the pulse width modulation (PWM) block input only for the boost mode. It is shown with dotted block in Figure 12.

4.2.2. Pulse Generation Logic

After the PWM generator generates the duty cycle for the main switch S_4 in the boost mode the gate pulses for the other switches are based on the logic as shown in Figure 13a, in tune with the waveforms for the boost mode. The switch S_6 operates complementary to switch S_4. So the pulse to it is through a NOT gate from S_4. Pulse to S_3 is after a time delay of $T_p/2$ from S_4. Switch S_5 receives a pulse complementary to S_3.

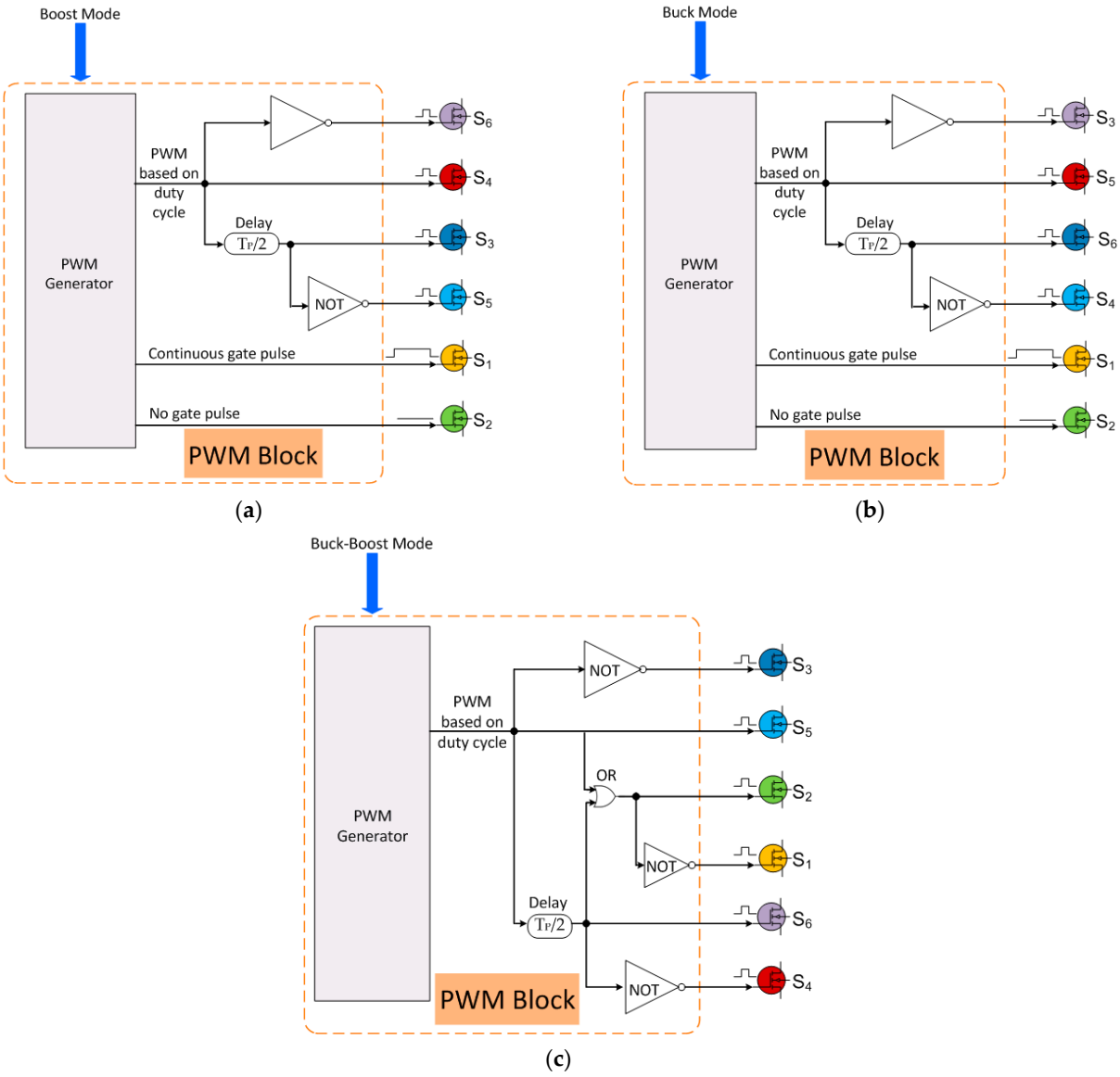

Figure 13. Logic for gate pulses based on duty cycle for main switches: (**a**) the boost mode; (**b**) the buck mode; (**c**) the buck-boost mode.

Similarly for the buck mode, the logic for the gate pulses is shown in Figure 13b.The switch S_3 operates complementary to switch S_5. So the pulse to it is through a NOT gate from S_5. Pulse to S_6 is after a time delay of $T_p/2$ from S_5. Switch S_4 receives a pulse complementary to S_6. The logic for the buck-boost mode is shown in Figure 13c. The switch S_3 operates complementary to main switch S_5. As shown NOT gate is used. Switch S_6 and

S_4 pulse logic is same as that for the buck mode. Switch S_2receivesa pulse only when either S_5 or S_6 is ON, hence it is through the OR gate. Switch S_1 receives a pulse complementary to S_2.

4.2.3. Mode Transition

When an EV is on a road, it is either driving or braking. The proposed converter has six modes transitions when switching from one operation to another. Table 2 lists the mode transitions as per the control logic in Figure 12. The gate pulse pattern for the switches will alter in accordance with the incoming mode when the converter transitions between modes. This is referred as mode transition. In Figure 14, the mode transition algorithm is displayed.

Table 2. Converter mode transitions during EV operation.

Vehicle Operation	Outgoing Mode	Incoming Mode
Driving to regenerative braking	Boost	Buck
	Boost	Buck-boost
Regenerative braking to driving	Buck	Boost
	Buck-boost	Boost
Regenerative braking	Buck	Buck-boost
	Buck-boost	Buck

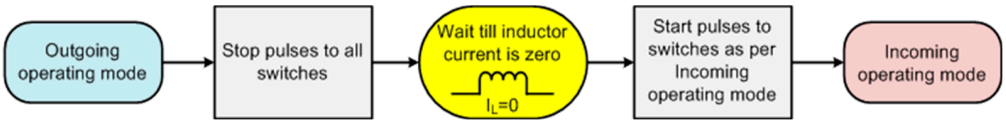

Figure 14. Mode transition algorithm.

The signal for mode transition is taken from the motor energy control unit based on the accelerator/brake pedal operation and control algorithm. Once the signal is received, the gate pulses to all the switches are blocked. The inductor current drops. After the inductor current reaches zero, the gate pulse pattern corresponding to the incoming mode comes into action. If the incoming mode is buck mode, then switch S_1 is activated first followed by switch S_5. All the other switches except switch S_2, will receive the pulses as per the logic shown in Figure 13b. Also for the boost mode, S_1 is operated first, followed by S_4. Switches S_3, S_5 and S_6 will receive pulses as per the logic shown in Figure 13a. Switch S_5 will be turned ON initially for the buck-boost mode. As per the logic in Figure 13c, all other switches will receivethe pulses.

The converter may enter the buck or buck-boost mode during regenerative braking, according to the voltage supplied by the traction machine. If the road is flat, the speed will drop as the braking advances, and the machine's voltage output will decrease. Therefore, if the converter had selected the buck mode at the start of braking, there is a chance that it could now switch to the buck-boost mode. This turns into the transition from the buck to the buck-boost mode in regenerative braking. Another instance is when the vehicle is moving downwards when the converter was initially in the buck-boost mode at the beginning of regenerative braking. The voltage may rise as the vehicle accelerates at a faster rate, causing the converter to switch to buck mode. The buck-boost to buck mode transition is seen in this case.

5. Results and Discussion

MATLAB/Simulink software (MATLAB 22a, MathWorks, Natick, MA, USA) is used to simulate both the proposed bidirectional dc–dc converter and the conventional half-bridge configuration based bidirectional dc–dc converter [31]. The simulations are carried out

to verify the proposed converter's performance during the normal drive operation of the vehicle corresponding to the boost mode of operation of the converter. The regenerative braking of the vehicle which corresponds to the buck and buck-boost modes of operation of the converter is simulated. The converter model for simulation is built as per the specifications given in Table 1 in Section 4.1. The simulations are run for 5 s. The purpose of the simulations is to compare and analyze the performance of the proposed converter.

5.1. Boost Mode Output

The input to the converter in this mode is the battery voltage. The battery rated voltage is 48 V, but depending upon the State of charge (SOC) it will range from 41 V to 54.6 V for the lithium-ion battery which is considered for the simulation. The output of the converter is the dc link voltage, which is 300 V for full speed of the vehicle. The same is the voltage for the inverter/traction motor.

Figure 15a shows the input and output voltage waveforms. The input voltage, V_b is 48 V and the reference voltage, and V_{dref} in the closed loop is set for 300 V. So the output voltage V_d obtained is 300 V. The next simulation is carried out with V_{dref} set to 250 V and then after 2 s changed to 280 V. As can be seen in Figure 15b, the boost mode gave the required output of 250 V initially and 280 V after 2 s. The gate pulses for the switches S_3, S_4, S_5, and S_6 are shown in Figure 15c corresponding to the output voltage of 300 V. S_3 and S_4 being the main switches for the boost action, their gate pulses are directly based on the duty cycle factor, $\delta = 0.68$; and as explained in Section 3.2.1 and shown in Figure 12, half the time period $T_p/2$ is added to it.

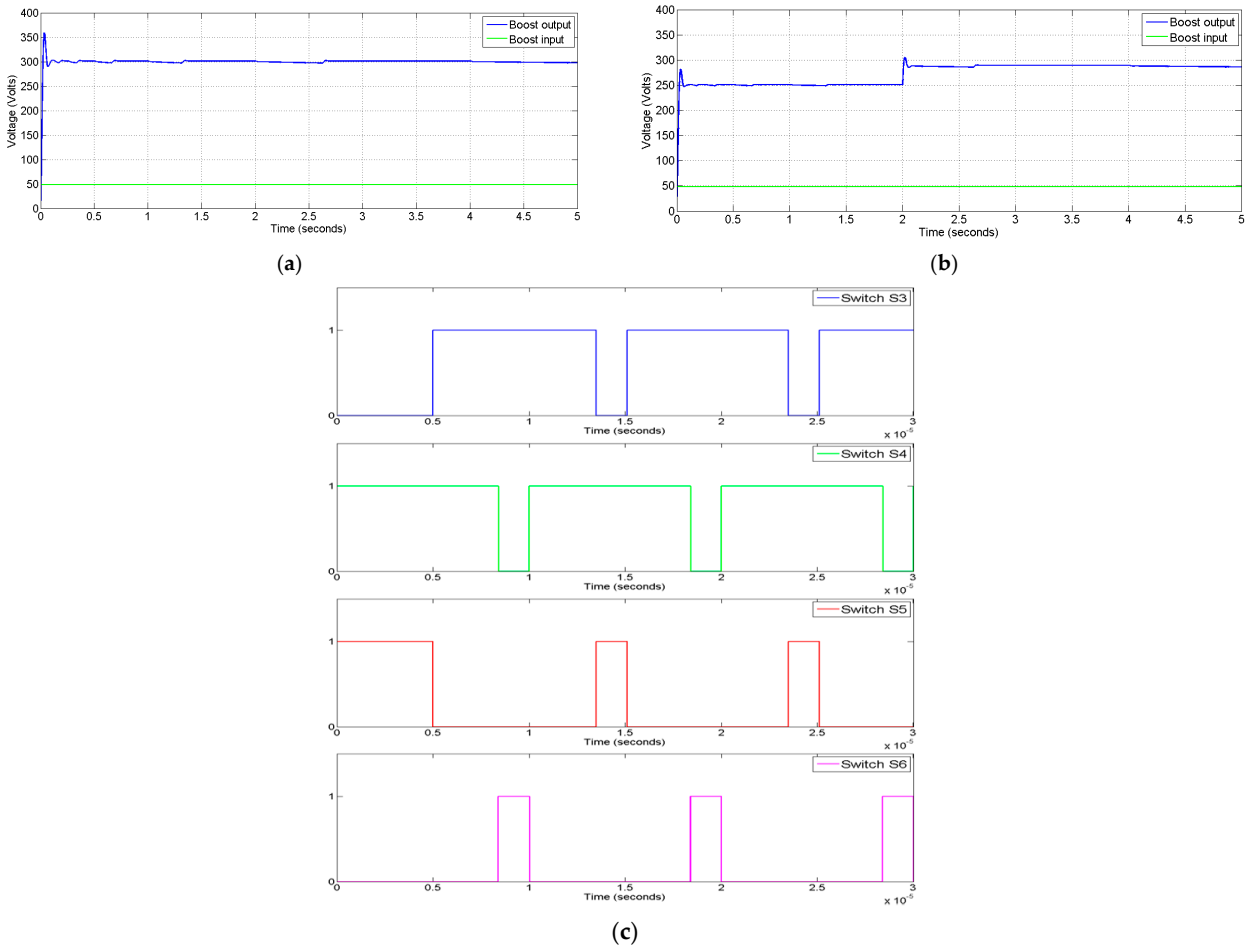

Figure 15. Waveforms for the boost mode: (**a**) input and output voltage when V_{dref} = 300 V; (**b**) input and output voltage when V_{dref} is changed from 250 V to 280 V; (**c**) gate pulses for switches S_3, S_4, S_5 and S_6 when V_{dref} = 300 V.

5.2. Buck Mode Output

The input to the converter in this mode is the dc link voltage. This is the voltage generated by the traction machine during regenerative braking. It will depend on the speed of the machine while regenerating. But for the battery to charge, it needs 56 to 56.8 V at its terminals. Considering 56 V as the output voltage of the buck mode V_b', the reference voltage, $V_b'_{ref}$ is set to 56 V.

For this mode, first the simulations are performed with the input voltage, V_d as 300 V and the reference voltage, $V_b'_{ref}$ in the closed loop set to 56 V. So the output voltage V_b' obtained is 56 V. This is seen in the waveforms in Figure 16a. Further simulation is carried out with input V_d kept at 120 V and after 2 s varied to 90 V from 2 s to 5 s. Consequently, the buck mode produced the necessary output of 56 V, as shown in Figure 16b. The gate pulses for the switches S_3, S_4, S_5, S_6 are shown in Figure 16c corresponding to the output voltage of 56 V with input voltage of 300 V. Since S_5 and S_6 are the primary switches for the buck action, the duty cycle factor, δ = 0.3734 directly determines the gate pulses for these switches.

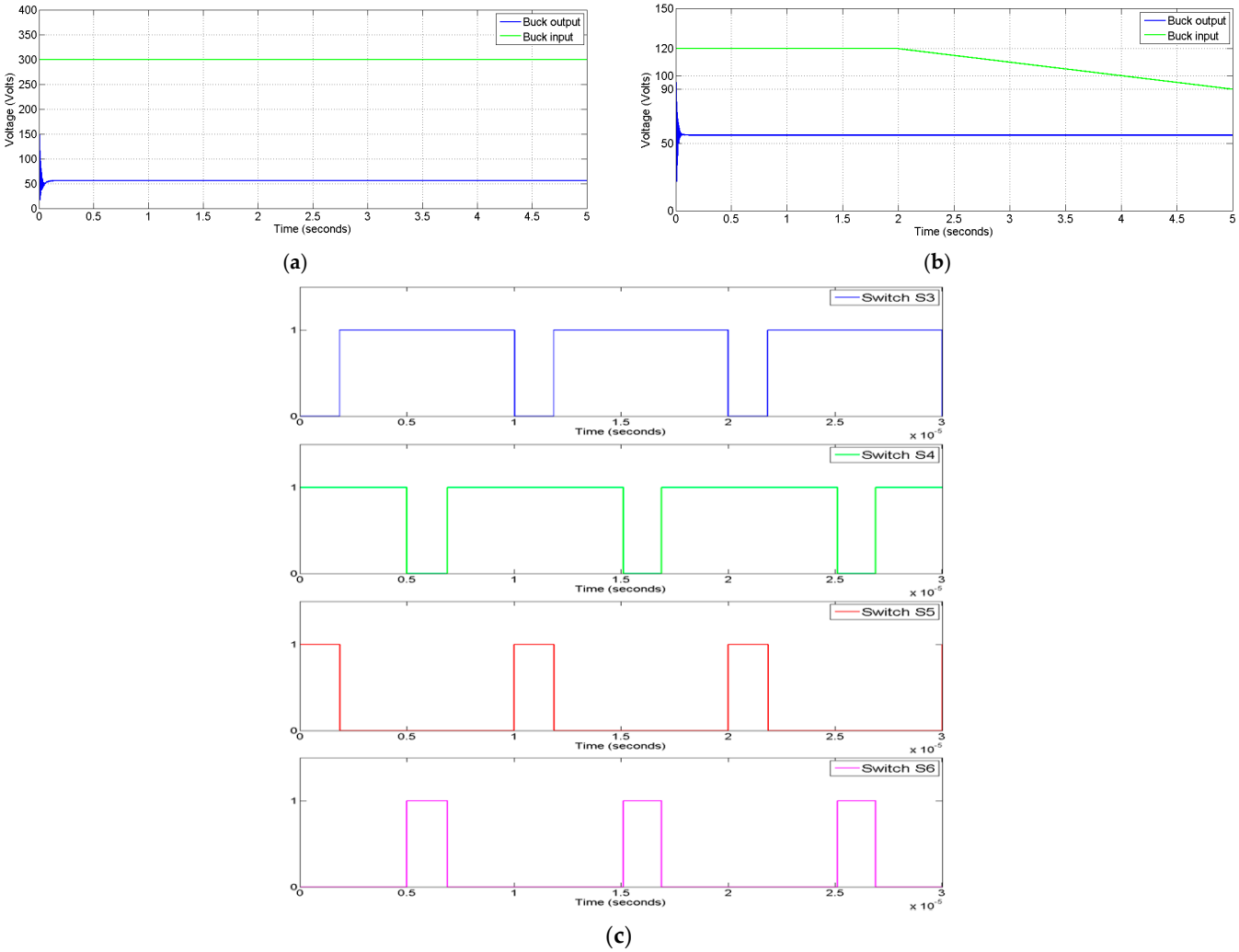

Figure 16. Waveforms for the buck mode: (**a**) input and output voltage when V_d = 300 V; (**b**) input and output voltage when V_d drops from 120 V to 90 V; (**c**) gate pulses for switches S_3, S_4, S_5 and S_6 when V_d = 300 V.

5.3. Buck-Boost Mode Output

Similar to the buck mode, this mode also comes into action during regenerative braking. The dc link voltage/generated voltage is the input to the converter for this mode.

This mode comes into action when the regenerated voltage V_d is less than or equal to twice the voltage required to charge the battery V_b'.

The first simulation is performed with input voltage of 90 V and after 2 s the voltage dropping from 90 V to 30 V within the next 3 s. As seen in Figure 17a, the buck-boost mode gave the required output of 56 V throughout. The buck action is seen till the input voltage varied from 90 V to 56 V and the boost action is noticed when the input voltage dropped below 56 V. The action changeover is seen at 3.7 s time in Figure 17a. The next simulation is with input voltage of 30 V rising to 90 V after 2 s within the next 3 s. The results are shown in Figure 17b and it is clear that the output voltage remains consistently 56 V.

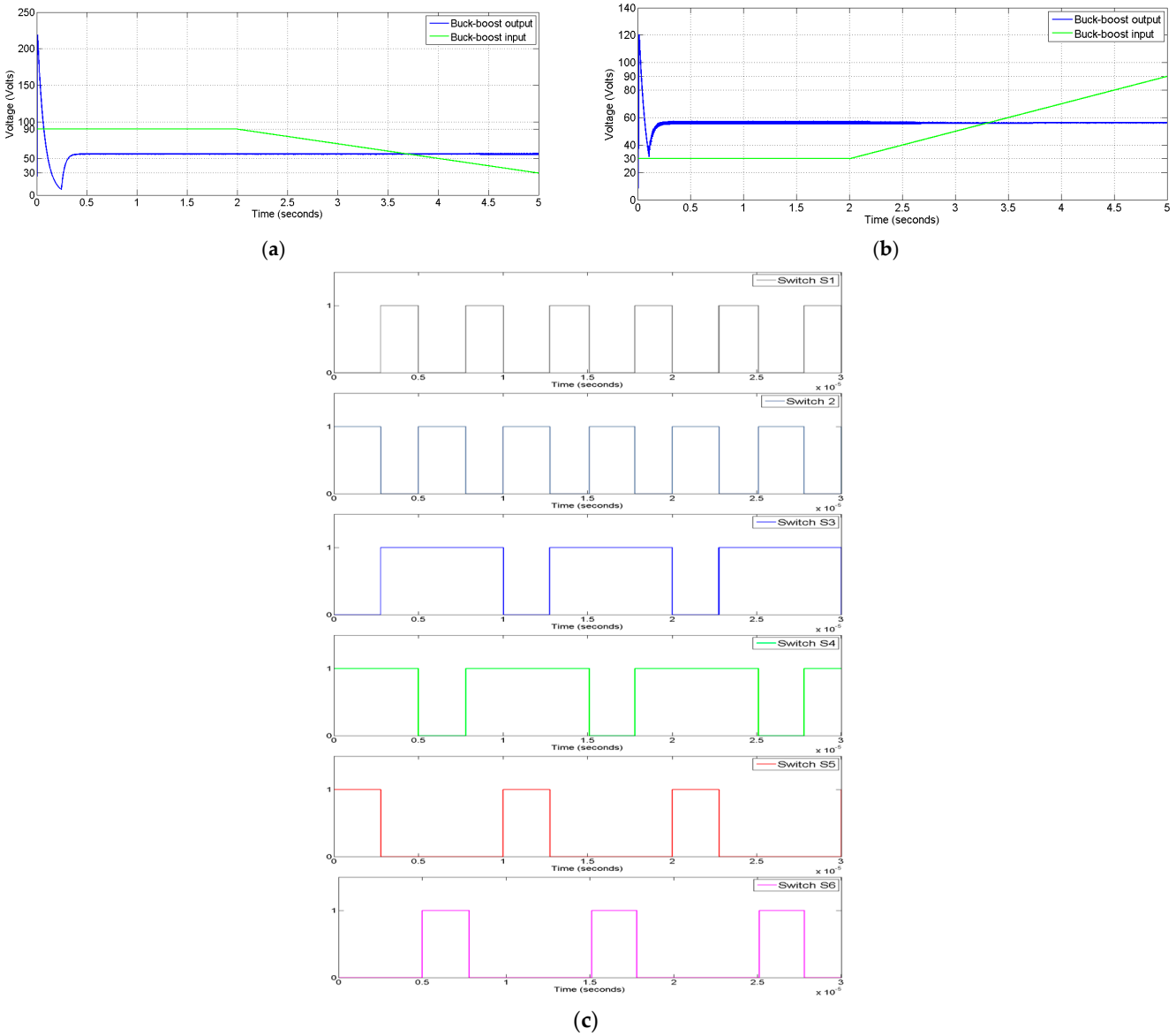

Figure 17. Waveforms for the buck-boost mode: (**a**) input and output voltage when V_d drops from 90 V to 30 V; (**b**) input and output voltage when V_d increases from 30 V to 90 V; (**c**) gate pulses for all the switches when V_d = 90 V.

The buck action comes into effect since the input voltage is above 56 V. Figure 17c displays the gate pulses for the switches S_1, S_2, S_3, S_4, S_5, S_6. These pulses correspond to an output voltage of 56 V and an input voltage of 90 V. Since S_5 and S_6 are the main switches for the buck-boost action, the gate pulses for these switches are directly determined by the duty cycle factor, δ = 0.5544.

Further the simulations are carried out in the similar way with the input voltage of 50 V slowly dropping to 30 V after 2 s as depicted in Figure 18a. Also the input voltage of 30 V slowly rises to 50 V, as seen in Figure 18b. In both these simulations, the boost action of this buck-boost mode comes into action to maintain the required voltage of 56 V at the output. The boost action is noticed in the beginning till 3.3 s after which the buck action comes into effect since the input voltage is above 56 V. For the switches S_1, S_2, S_3, S_4, S_5, and S_6, the gate pulses are displayed in Figure 18c, which corresponds to an output voltage of 56 V with an input voltage of 30 V. The duty cycle factor, $\delta = 0.7887$, directly defines the gate pulses for S_5 and S_6, which are the main switches for the buck-boost action.

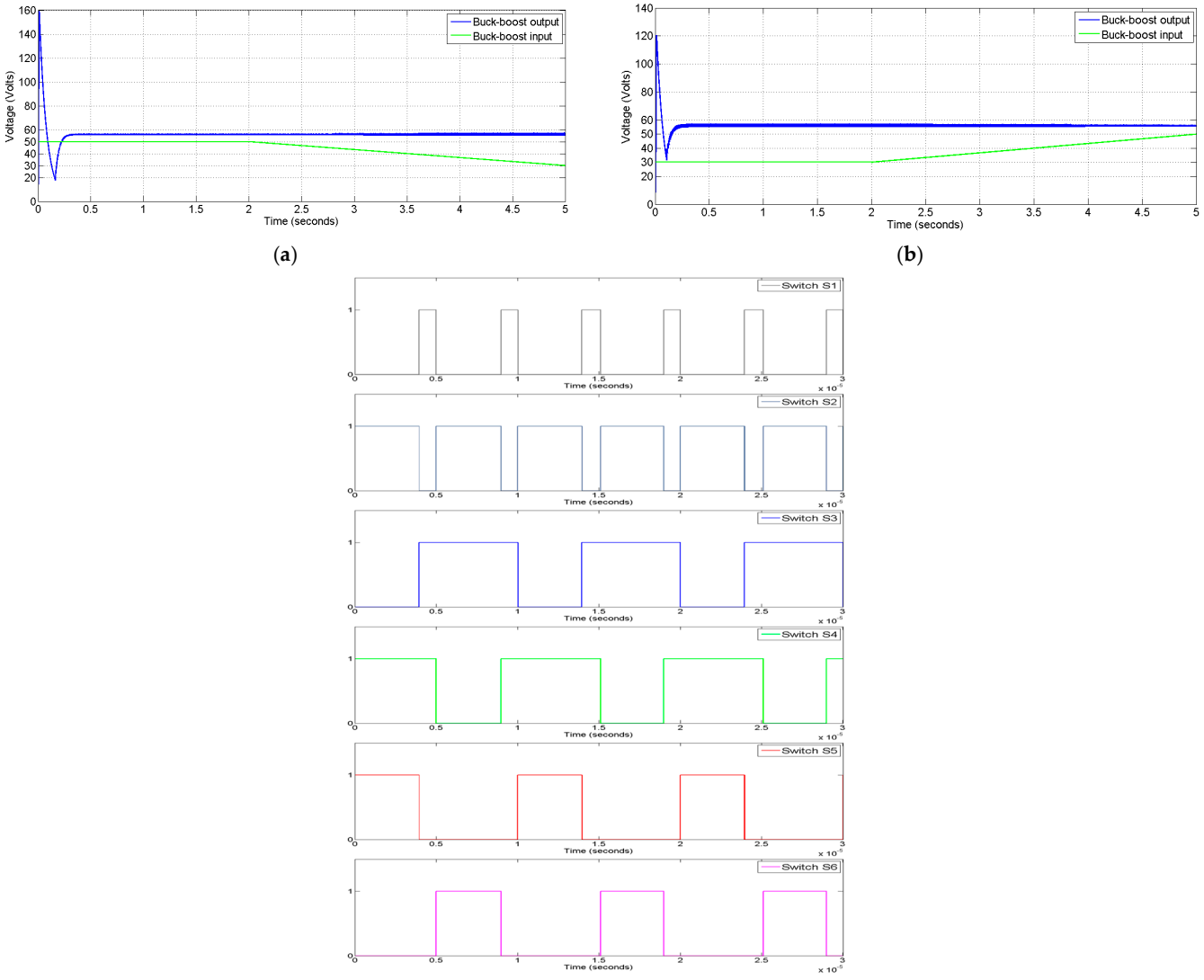

Figure 18. Waveforms for the buck-boost mode: (**a**) input and output voltage when V_d drops from 50 V to 30 V; (**b**) input and output voltage when V_d increases from 30 V to 50 V; (**c**) gate pulses for all the switches when V_d = 30 V.

5.4. Mode Transition Output

Simulation for mode transition carried out considering that the vehicle is in propulsion with the converter in the boost mode giving dc link voltage of 300 V. At 2.5 s, regenerative braking is applied and the converter power flow reverses. The converter which is now operating in the buck mode gives an output voltage of 56 V to charge the battery. This is depicted in Figure 19a. The inductor current during mode transition is highlighted in Figure 19b. During the transition from the boost mode to the buck mode, the inductor

current direction reverses. The buck mode is initiated only after the inductor current reaches zero.

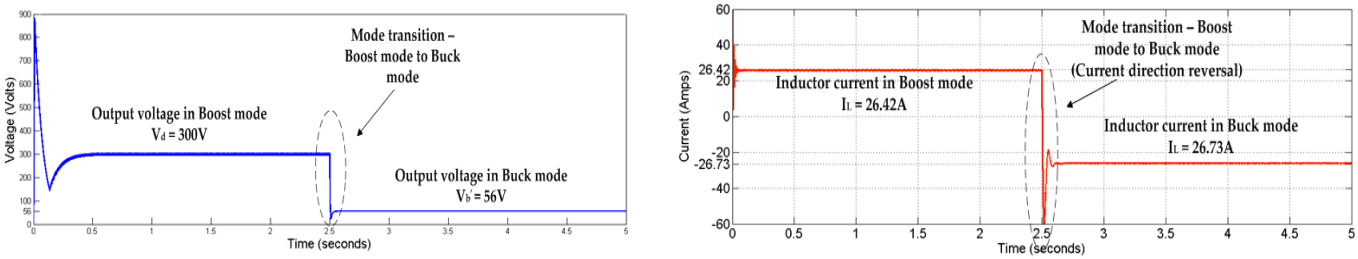

(**a**) (**b**)

Figure 19. Waveforms during mode transition from the boost mode to the buck mode. (**a**) Output voltages; (**b**) inductor current.

Figure 20a brings out the comparison of voltage gain against duty cycle between the proposed converter and the conventional converter. The voltage gain of the proposed converter is double as compared with the conventional converter for the same duty cycle factor. 300 V output for the boost mode was obtained with $\delta = 0.68$ for proposed converter. But conventional converter requires $\delta = 0.84$ to obtain the same output voltage. Also for the buck mode, as seen in Figure 20b, to obtain an output voltage of 56 V from 300 V input, the duty cycle factor required is $\delta = 0.3734$ for proposed converter as against $\delta = 0.1867$ for the conventional converter. This confirms that the voltage gain is half for the proposed converter compared to the conventional one.

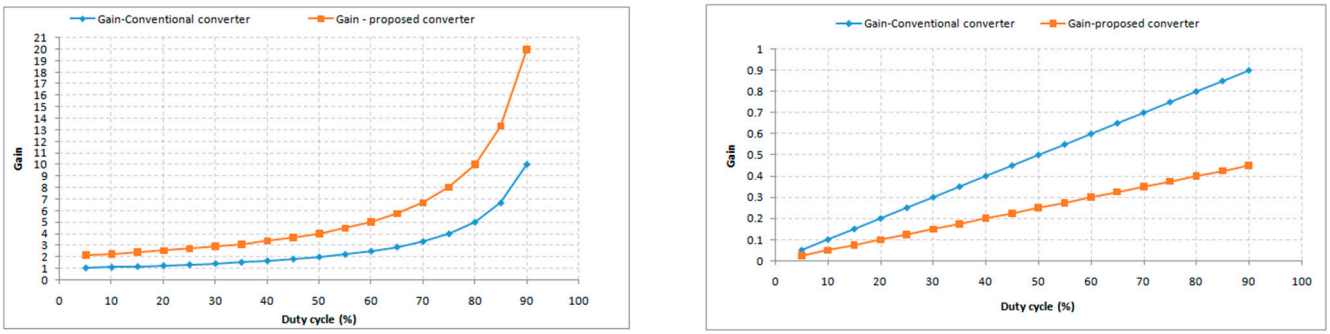

(**a**) (**b**)

Figure 20. Comparison of voltage gain against duty cycle between proposed converter and conventional converter for (**a**) the boost mode; (**b**) the buck mode.

The voltage gain against duty cycle for the buck and buck-boost modes for the proposed converter is shown in Figure 21. With the condition for the selection of the buck or buck-boost mode for regenerative braking, the buck mode will provide the required voltage of 56 V at output for input voltage above 112 V. With the input voltage nearing 112 V, δ reaches close to 1 as against 0.5 for the conventional converter. Voltages equal to and below 112 V are handled by the buck-boost mode. When the input voltage is in the range above 56 V to 112 V, the buck action of the buck-boost mode comes into effect. Input voltages below 56 V are handled by the boost action of the buck-boost mode. This is tabulated in Table 3.

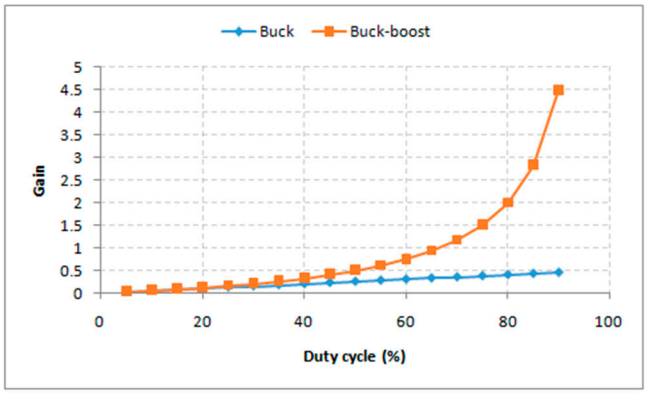

Figure 21. Voltage gain against duty cycle for the buck and buck-boost modes of the proposed converter.

Table 3. Regenerative braking voltage and corresponding operating mode.

Generated Voltage	Operating Mode	
Above $2V_b'$ up to V_d (max)	Buck mode	
Above V_b' up to $2V_b'$	Buck-boost mode	Buck action
V_b' and below		Boost action

Table 4 is a comparative table that illustrates the superiority of the novel proposed converter over the half-bridge based converter. The comparison is based on several factors including the number of modes of operation, voltage gain in the boost mode, voltage range, and voltage stress on the switches and cost. The first four factors reveal the benefits of the proposed converter. The cost of the proposed converter is comparatively more than the half-bridge based converter due to the utilization of four additional switches and implementation of the control logic. Comparison of proposed converter with the available converters in the literature is shown in Table 5. The comparison is specific for the EV application. Due to the use of both the buck and buck-boost modes during regenerative braking, this novel configuration makes it possible for power to flow from the traction machine to the battery even if the regenerated voltage is lower than the voltage required for charging the battery. This unique feature makes it a favorable topology for EV application.

Table 4. Comparison of proposed bidirectional converter with conventional half-bridge bidirectional configuration for EV.

Feature/Parameter	Half-Bridge Converter	Proposed Converter
Modes of operation	Buck, boost	Buck, boost and Buck-boost
Voltage gain in boost mode	Normal	Double
Voltage range	Normal	Wide
Voltage stress on switches	High-side voltage	Half the high-side voltage
Cost	Low cost	Additional cost

Table 5. Comparison of proposed bidirectional converter with all other bidirectional configuration in the literature for EV application.

Feature	Other Converter Configurations in Literature	Proposed Converter
Potential to use regenerative energy at low braking speeds when the voltage generated is less than that needed to charge the battery.	No	Yes

6. Conclusions

This research paper introduces atri-mode dc–dc non-isolated bidirectional converter designed to address the limitations associated with a wide voltage range for precise speed control and the recovery of regenerative braking energy at low speeds in electric vehicles. This novel converter is based on the modified version of the conventional bidirectional buck and boost converter and incorporates additional switches. It operates in three modes: buck, boost and buck-boost. An in-depth analysis of the converter operation for all the three modes with theoretical waveforms incorporating PWM switching is provided. A novel closed loop control strategy with pulse generation logic for all the switches is presented. An algorithm for mode transition is developed in order to influence the pulse pattern when changing over between modes.

Results show that the proposed novel converter provides double the voltage gain with a broad voltage range in the boost mode during running. During regenerative braking, the converter switches between the buck and buck-boost modes based on the voltage generated by the traction machine and a control algorithm. It acts as a buck converter when the generated voltage exceeds double the battery charging requirement and switches to the buck-boost mode when the voltage falls short. This mode-switching feature helps to maintain the required voltage for battery charging for all braking speeds. The configuration also reduces the voltage stress on the switches to half the dc link voltage.

The results confirm the converter's functionality. Thus, for electric vehicles with bidirectional buck and a boost converter between battery and the traction motor/inverter, the proposed tri-mode converter can be a promising topology for enhancing regenerative braking efficiency and fine speed control of the vehicle during running.

Author Contributions: Conceptualization, N.D. and A.J.N.; methodology, software and validation, N.D., A.J.N. and V.N.S.; formal analysis, investigation, resources, writing—original draft preparation, writing—review and editing, visualization, supervision and project administration, N.D., A.J.N. and V.N.S. All authors have read and agreed to the published version of the manuscript.

Funding: This research received no external funding.

Data Availability Statement: Data are contained within this article.

Conflicts of Interest: The authors declare no conflict of interest.

References

1. Fathabadi, H. Utilizing solar and wind energy in plug-in hybrid electric vehicles. *Energy Convers. Manag.* **2018**, *156*, 317–328. [CrossRef]
2. Gua, C.; Chan, C.C. Whole-system thinking, development control, key barriers and promotion mechanism for EV development. *J. Mod. Power Syst. Clean Energy* **2015**, *3*, 160–169. [CrossRef]
3. Rajashekara, K. Present status and future trends in Electric vehicle propusion technologies. *IEEE Trans. Emerg. Sel. Topics Power Electron.* **2013**, *1*, 3–10. [CrossRef]
4. De Santis, M.; Silvestri, L.; Forcina, A. Promoting electric vehicle demand in Europe: Design of innovative electricity consumption simulator and subsidy strategies based on well-to-wheel analysis. *Energy Convers. Manag.* **2022**, *270*, 116279. [CrossRef]
5. Abas, A.P.; Yong, J.E.; Mahlia, T.M.; Hannan, M.A. Techno-economic analysis and environmental impact of electric vehicle. *IEEE Access* **2019**, *7*, 98565–98578. [CrossRef]
6. Liu, C.; Chau, K.T.; Wu, D. Opportunities and challenges of vehicle-to-home, vehicle-to-vehicle, and vehicle-to-grid technologies. *Proc. IEEE.* **2013**, *11*, 2409–2427. [CrossRef]
7. Lai, C.S.; Jia, Y.; Dong, Z.; Wang, D.; Tao, Y.; Lai, Q.H.; Wong, R.T.K.; Zobaa, A.F.; Wu, R.; Lai, L.L. A review of technical standards for smart cities. *Clean Technol.* **2020**, *2*, 290–310. [CrossRef]
8. Tran, M.K.; Bhatti, A.; Vrolyk, R.; Wong, D.; Panchal, S.; Fowler, M.; Fraser, R. A review of range extenders in battery electric vehicles: Current progress and future perspectives. *World Electr. Veh. J.* **2021**, *12*, 54. [CrossRef]
9. Tu, H.; Feng, H.; Srdic, S.; Lukic, S. Extreme fast charging of electric vehicles: A technology overview. *IEEE Trans. Transp. Electrif.* **2019**, *5*, 861–878. [CrossRef]
10. Kosuru, V.S.; Kavasseri Venkitaraman, A. A Smart Battery Management System for Electric Vehicles Using Deep Learning-Based Sensor Fault Detection. *World Electr. Veh. J.* **2023**, *14*, 101. [CrossRef]
11. Bagchi, A.C.; Kamineni, A.; Zane, R.A.; Carlson, R. Review and comparative analysis of topologies and control methods in dynamic wireless charging of electric vehicles. *IEEE Trans. Emerg. Sel. Top. Power Electron.* **2021**, *9*, 4947–4962. [CrossRef]

12. Maroti, P.K.; Padmanaban, S.; Bhaskar, M.S.; Ramachandaramurthy, V.K.; Blaabjerg, F. The state-of-the-art of power electronics converters configurations in electric vehicle technologies. *Power Electron. Dev. Compon.* **2022**, *1*, 100001. [CrossRef]
13. Shenai, K. High-density power conversion and wide-bandgap semiconductor power electronics switching devices. *Proc. IEEE.* **2019**, *107*, 2308–2326. [CrossRef]
14. Sladic, S.; De Santis, M.; Zivic, E.; Giemacki, W. Paradigm Changes in Power Electronics Caused by Emerging Materials. In Proceedings of the IEEE International Congress on Advanced Materials Sciences and Engineering (AMSE), Opatija, Crotia, 22 July 2022.
15. Nguyen, H.V.; Lee, D.C.; Blaabjerg, F. A novel SiC-based multifunctional onboard battery charger for plug-in electric vehicles. *IEEE Trans. Power Electron.* **2020**, *36*, 5635–5646. [CrossRef]
16. Naradhipa, A.M.; Kim, S.; Yang, D.; Choi, S.; Yeo, I.; Lee, Y. Power density optimization of 700 kHz GaN-based auxiliary power module for electric vehicles. *IEEE Trans. Power Electron.* **2020**, *36*, 5610–5621. [CrossRef]
17. Xing, Y.; Lv, C. Dynamic state estimation for the advanced brake system of electric vehicles by using deep recurrent neural networks. *IEEE Trans. Ind. Electron.* **2019**, *67*, 9536–9547. [CrossRef]
18. Yang, C.; Zha, M.; Wang, W.; Liu, K.; Xiang, C. Efficient energy management strategy for hybrid electric vehicles/plug-in hybrid electric vehicles: Review and recent advances under intelligent transportation system. *IET Intell. Transp. Syst.* **2020**, *14*, 702–711. [CrossRef]
19. Habib, S.; Khan, M.M.; Abbas, F.; Ali, A.; Faiz, M.T.; Ehsan, F.; Tang, H. Contemporary trends in power electronics converters for charging solutions of electric vehicles. *CSEE J. Power Energy Syst.* **2020**, *6*, 911–929.
20. Macharia, V.M.; Garg, V.K.; Kumar, D. A review of electric vehicle technology: Architectures, battery technology and its management system, relevant standards, application of artificial intelligence, cyber security, and interoperability challenges. *IET Electr. Syst. Transp.* **2023**, *13*, e12083. [CrossRef]
21. Zgheib, R.; Kamwa, I.; Al-Haddad, K. Comparison between isolated and non-isolated DC/DC converters for bidirectional EV chargers. In Proceedings of the IEEE International Conference on Industrial Technology (ICIT), Toronto, ON, Canada, 22 March 2017.
22. Tendillo, L.A. Design and Control of a Bidirectional DC/DC Converter for an Electric Vehicle Application. Ph.D. Thesis, Universitat Rovira I Virgili, Tarragona, Spain, 2015.
23. Dong, Z.; Joung, G. Soft-Switched Synchronous Buck Converter for Battery Chargers. *Int. J. Adv. Smart Converg.* **2019**, *8*, 138–146.
24. Dave, M.R.; Dave, K.C. Analysis of boost converter using PI control algorithms. *Int. J. Eng. Trends Technol.* **2012**, *3*, 71–73.
25. Qiao, H.; Zhang, Y.; Yao, Y.; Wei, L. Analysis of buck-boost converters for fuel cell electric vehicles. In Proceedings of the IEEE International Conference on Vehicular Electronics and Safety, Shanghai, China, 13 December 2006.
26. Poorali, B.; Adib, E.; Farzanehfard, H. Soft-switching DC–DC Cuk converter operating in discontinuous-capacitor-voltage mode. *IET Power Electron.* **2017**, *10*, 1679–1686. [CrossRef]
27. Siddharthan, N.; Balasubramanian, B. Performance evaluation of SEPIC, Luo and ZETA converter. *Int. J. Power Electron. Drive Syst.* **2019**, *10*, 374. [CrossRef]
28. Adlakha, R.; Khosla, A.; Joshi, D. Comparative analysis of positive output super lift DC–DC luo converters. *Indones. J. Electr. Eng. Comput. Sci.* **2020**, *18*, 707–716. [CrossRef]
29. Narasipuram, R.P. Analysis, identification and design of robust control techniques for ultra-lift Luo DC–DC converter powered by fuel cell. *Int. J. Comput. Aided Eng. Technol.* **2021**, *14*, 102–129. [CrossRef]
30. Pascual, C.; Krein, P.T. Switched capacitor system for automatic series battery equalization. In Proceedings of the IEEE Conference on Applied Power Electronics Conference and Exposition (APEC), Vancouver, BC, Canada, 27 February 1997.
31. Tesla Blog. Available online: https://www.tesla.com/blog (accessed on 3 October 2023).
32. Audi Mediacenter. Available online: https://www.audi-mediacenter.com/en (accessed on 3 October 2023).
33. Porsche Newsroom. Available online: https://newsroom.porsche.com/en/products/taycan/battery-18557.html (accessed on 3 October 2023).
34. Anbazhagan, L.; Ramiah, J.; Krishnaswamy, V.; Jayachandran, D.N. A comprehensive review on Bidirectional traction converter for Electric vehicles. *Int. J. Electron. Telecommun.* **2019**, *65*, 635–649.
35. Kang, T.; Kim, C.; Suh, Y.; Park, H. A design and control of bi-directional non-isolated DC–DC converter for rapid electric vehicle charging system. In Proceedings of the 27th Annual IEEE Applied Power Electronics Conference and Exposition, Orlando, FL, USA, 5–9 February 2012.
36. Wai, R.J.; Duan, R.Y.; Jheng, K.H. High-efficiency bidirectional dc–dc converter with high-voltage gain. *IET Power Electron.* **2012**, *5*, 173–184. [CrossRef]
37. Hsieh, Y.P.; Chen, J.F.; Yang, L.S.; Wu, C.Y.; Liu, W.S. High-conversion-ratio bidirectional DC–DC converter with coupled inductor. *IEEE Trans. Ind. Electron.* **2013**, *61*, 210–222. [CrossRef]
38. Beraki, M.W.; Trovão, J.P.; Perdigão, M.S.; Dubois, M.R. Variable inductor based bidirectional DC–DC converter for electric vehicles. *IEEE Trans. Veh. Technol.* **2017**, *66*, 8764–8772. [CrossRef]
39. Hosseinzadeh, Z.; Molavi, N.; Farzanehfard, H. Soft-switching high step-up/down bidirectional DC–DC converter. *IEEE Trans. Ind. Electron.* **2018**, *66*, 4379–4386. [CrossRef]
40. Zhang, Y.; Liu, H.; Li, J.; Sumner, M. A low-current ripple and wide voltage-gain range bidirectional DC–DC converter with coupled inductor. *IEEE Trans. Power Electron.* **2019**, *35*, 1525–1535. [CrossRef]

41. Malik, M.Z.; Zhang, S.; Hong, Y.; Alwahkyan, A.R.; Ali, A.; Farooq, A. A Coupled Inductor-Based Bidirectional DC–DC Converter with Step-Up Step-Down Operation for Electric Vehicle Applications. *Int. Trans. Electr. Energy Syst.* **2023**, *2023*, 9277881. [CrossRef]
42. Cortez, D.F.; Waltrich, G.; Fraigneaud, J.; Miranda, H.; Barbi, I. DC–DC converter for dual-voltage automotive systems based on bidirectional hybrid switched-capacitor architectures. *IEEE Trans. Ind. Electrons.* **2014**, *62*, 3296–3304. [CrossRef]
43. Choi, H.; Jang, M.; Agelidis, V.G. Zero-current-switching bidirectional interleaved switched-capacitor DC–DC converter: Analysis, design and implementation. *IET Power Electron.* **2016**, *9*, 1074–1082. [CrossRef]
44. Li, S.; Smedley, K.M.; Caldas, D.R.; Martins, Y.W. Hybrid bidirectional DC–DC converter with low component counts. *IEEE Trans. Ind. Appl.* **2017**, *54*, 1573–1582. [CrossRef]
45. Zhang, Y.; Gao, Y.; Zhou, L.; Sumner, M. A switched-capacitor bidirectional DC–DC converter with wide voltage gain range for electric vehicles with hybrid energy sources. *IEEE Trans. Power Electron.* **2018**, *33*, 9459–9469. [CrossRef]
46. Zhang, Y.; Liu, Q.; Gao, Y.; Li, J.; Sumner, M. Hybrid switched-capacitor/switched-quasi-Z-source bidirectional DC–DC converter with a wide voltage gain range for hybrid energy sources EVs. *IEEE Trans. Ind. Electron.* **2018**, *66*, 2680–2690. [CrossRef]
47. Zhang, Y.; Zhang, W.; Gao, F.; Gao, S.; Rogers, D. A switchedcapacitor interleaved bidirectional converter with wide voltage-gain range for super capacitors in EVs. *IEEE Trans. Power Electron.* **2020**, *35*, 1536–1547. [CrossRef]
48. Rezaii, R.; Nilian, M.; Safayatullah, M.; Ghosh, S.; Batarseh, I. A Bidirectional DC–DC Converter with High Conversion Ratios for the Electrical Vehicle Application. In Proceedings of the 47th Annual Conference of the IEEE Industrial Electronics Society, Toronto, ON, Canada, 13–15 October2021.
49. Ardi, H.; Ajami, A.; Kardan, F.; Avilagh, S.N. Analysis and implementation of a nonisolated bidirectional DC–DC converter with high voltage gain. *IEEE Trans Ind. Electron.* **2016**, *63*, 4878–4888.
50. Elsayad, N.; Moradisizkoohi, H.; Mohammed, O.A. A new hybrid structure of a bidirectional DC–DC converter with high conversion ratios for electric vehicles. *IEEE Trans. Veh. Technol.* **2019**, *69*, 194–206. [CrossRef]
51. Jiang, F.; Wang, P.; Wang, Z.; Deng, Q.; Li, B.; Tao, L.; Cheng, Z. A Zero Current Ripple Bidirectional DC–DC Converter with High Voltage Gain and Common Ground for Hybrid Energy Storage System EVs. *IEEE Trans. Emerg. Sel. Top. Power Electron.* **2023**, *11*, 4882–4894. [CrossRef]
52. Sojoudi, T.; Sarhangzadeh, M.; Olamaei, J.; Ardashir, J.F. An Extendable Bidirectional High Gain DC–DC Converter for Electric Vehicle Applications Equipped with IOFL Controller. *IEEE Trans. Power Electron.* **2023**, *38*, 9767–9779. [CrossRef]
53. Zhang, Y.; Gao, Y.; Li, J.; Sumner, M. Interleaved switched-capacitor bidirectional DC–DC converter with wide voltage-gain range for energy storage systems. *IEEE Trans. Power Electron.* **2017**, *33*, 3852–3869. [CrossRef]
54. Bahrami, H.; Farhangi, S.; Iman-Eini, H.; Adib, E. A new interleaved coupled-inductor nonisolated soft-switching bidirectional DC–DC converter with high voltage gain ratio. *IEEE Trans. Ind. Electron.* **2017**, *65*, 5529–5538. [CrossRef]
55. Rathore, V.; Rajashekara, K.; Nayak, P.; Ray, A. A High-Gain Multilevel dc–dc Converter for Interfacing Electric Vehicle Battery and Inverter. *IEEE Trans. Ind. Appl.* **2022**, *58*, 6506–6518. [CrossRef]
56. De Melo, R.R.; Tofoli, F.L.; Daher, S.; Antunes, F.L. Interleaved bidirectional DC–DC converter for electric vehicle applications based on multiple energy storage devices. *Electr. Eng.* **2020**, *102*, 2011–2023. [CrossRef]
57. Konjedic, T.; Korošec, L.; Truntič, M.; Restrepo, C.; Rodič, M.; Milanovič, M. DCM-based zero-voltage switching control of a bidirectional DC–DC converter with variable switching frequency. *IEEE Trans. Power Electron.* **2015**, *31*, 3273–3288. [CrossRef]
58. Chen, J.; Sha, D.; Yan, Y.; Liu, B.; Liao, X. Cascaded high voltage conversion ratio bidirectional nonisolated DC–DC converter with variable switching frequency. *IEEE Trans. Power Electron.* **2017**, *33*, 1399–1409. [CrossRef]
59. Das, P.; Laan, B.; Mousavi, S.A.; Moschopoulos, G. A nonisolated bidirectional ZVS-PWM active clamped DC–DC converter. *IEEE Trans. Power Electron.* **2009**, *24*, 553–558. [CrossRef]
60. Das, P.; Mousavi, S.A.; Moschopoulos, G. Analysis and Design of a Nonisolated Bidirectional ZVS-PWM DC–DC Converter with Coupled Inductors. *IEEE Trans. Power Electron.* **2010**, *25*, 2630–2641. [CrossRef]
61. Lee, Y.S.; Ko, Y.P.; Cheng, M.W.; Liu, L.J. Multiphase zero-current switching bidirectional converters and battery energy storage application. *IEEE Trans. Power Electron.* **2012**, *28*, 3806–3815. [CrossRef]
62. Jiang, L.; Mi, C.C.; Li, S.; Zhang, M.; Zhang, X.; Yin, C. A novel soft-switching bidirectional DC–DC converter with coupled inductors. *IEEE Trans. Ind. Appl.* **2013**, *49*, 2730–2740. [CrossRef]
63. Kwon, M.; Oh, S.; Choi, S. High gain soft-switching bidirectional DC–DC converter for eco-friendly vehicles. *IEEE Trans. Power Electron.* **2013**, *29*, 1659–1666. [CrossRef]
64. Yang, J.W.; Do, H.L. High-efficiency bidirectional dc–dc converter with low circulating current and ZVS characteristic throughout a full range of loads. *IEEE Trans Ind. Electron.* **2013**, *61*, 3248–3256. [CrossRef]
65. Yang, J.W.; Do, H.L. Soft-Switching Bidirectional DC–DC Converter Using a Lossless Active Snubber. *IEEE Trans. Circuits Syst. IRegul. Pap.* **2014**, *61*, 1588–1596. [CrossRef]
66. Aamir, M.; Mekhilef, S.; Kim, H.J. High-gain zero-voltage switching bidirectional converter with a reduced number of switches. *IEEE Trans. Circuits Syst. II Express Briefs.* **2015**, *62*, 816–820. [CrossRef]
67. Dusmez, S.; Khaligh, A.; Hasanzadeh, A. A zero-voltage-transition bidirectional DC/DC converter. *IEEE Trans. Ind. Electron.* **2015**, *62*, 3152–3162. [CrossRef]
68. Ashique, R.H.; Salam, Z. A family of true zero voltage zero current switching (ZVZCS) nonisolated bidirectional DC–DC converter with wide soft switching range. *IEEE Trans. Ind. Electron.* **2017**, *64*, 5416–5427. [CrossRef]

69. Molavi, N.; Adib, E.; Farzanehfard, H. Soft-switching bidirectional DC–DC converter with high voltage conversion ratio. *IET Power Electron.* **2018**, *11*, 33–42. [CrossRef]
70. Ashique, R.H.; Salam, Z. A high-gain, high-efficiency nonisolated bidirectional DC–DC converter with sustained ZVS operation. *IEEE Trans. Ind. Electron.* **2018**, *65*, 7829–7840. [CrossRef]
71. Zhang, Y.; Cheng, X.F.; Yin, C.; Cheng, S. Analysis and research of a soft-switching bidirectional DC–DC converter without auxiliary switches. *IEEE Trans. Ind. Electron.* **2017**, *65*, 1196–1204. [CrossRef]
72. Wang, H.; Guo, J.; Gong, J.; Chen, J.; Zhang, S. The Impact of Dead-time on Synchronous Rectification Circuit Efficiency. In Proceedings of the International Conference on Wireless Communication, Network and Multimedia Engineering, Guilin, China, 21–22 April 2019.
73. Panigrahi, R.; Mishra, S.K.; Joshi, A.; Ngo, K.D. Synthesis of DC–DC Converters from Voltage Conversion Ratio and Prescribed Requirements. *IEEE Trans. Power Electron.* **2021**, *36*, 13889–13902. [CrossRef]
74. Pressman, A.I.; Billings, K.; Morey, T. *Switching Power Supply Design*, 3rd ed.; The McGraw-Hill Companies: New York, NY, USA, 2009; pp. 21–30, 33–37.
75. Li, S.; Jiang, Q. Study on pid parameters tuning method based on Matlab/Simulink. In Proceedings of the IEEE 3rd Conference on Communication Software and Networks, Xian, China, 27–29 May 2011.